THE DYNAMIC IMPACTS OF ELECTRIC VEHICLE INTEGRATION ON THE ELECTRICITY DISTRIBUTION GRID

by

RUI SHI

A thesis submitted to
The University of Birmingham
for the degree of
MASTER OF PHILOSOPHY

School of Electronic,
Electrical and Computer Engineering
The University of Birmingham
November 2012

To my parents

ACKNOWLEDGEMENTS

First and foremost, I would like to express my sincere appreciation to my supervisor, Professor Xiao-Ping Zhang, for his support, guidance, inspiration and patience during my study. I have greatly benefited from his knowledge and experience.

I am also grateful to Dr. Gan Li and Dr. Dechao Kong for their support and advices on my research. Many thanks to Mr. Zhou Li and Mr. Xuan Yang, Mr. Suyang Zhou for sharing their valuable ideas with me. I would also like to thank my dear colleagues Miss Na Deng, Mr. Jingchao Deng, Mr. Puyu Wang, and Mr. Jianing Li for their discussions and kind assistance during my study.

Finally, I would like to thank my families and all my friends. Without their encouragement, support and understanding, completion of my thesis would not be possible.

ABSTRACT

This thesis is mainly concerned with the modeling of electric vehicle charging station and its dynamic interactions with distribution grid.

The thesis starts with the literature review of the technical developments in wind generation and electric vehicle integration into power grids. Then the equivalent model of electric batteries is developed and implemented in MATLAB/Simulink. The model is used to evaluate the terminal voltage and power variation during the battery charging and discharging periods. The concept of electric vehicle fast charging station is summarized and its detailed simulation model is designed for the integration of the electric vehicle batteries with the distribution network. In addition, the modeling of a wind turbine with DFIG is presented. As a wind generator requires the fault ride-through ability, crowbar protection is considered in the simulation model.

Based on the above, the interactions between electric vehicle charging stations and active distribution grid with wind turbines are investigated. The focus is to examine the possibility of bi-direction power flow control capability of EV charging stations in providing the voltage support for distribution network operations to improve the fault-ride-through of adjacent wind turbines. Simulations are used to illustrate the feasibility as well as the effectiveness of the proposed control concept. Potentially such voltage support from EV charging station can be developed as ancillary services in smart distribution grid operations.

TABLE OF CONTENTS

LIST OF FIGURES

Chapter 1 Introduction

Abstract

In this Chapter, the motivation for the research topics of this thesis on the dynamic impacts of electric vehicles on the distribution grid is presented at first. Then a literature review is carried out on research topics of electric vehicles and wind generation as well as their current developments. Finally the organization of this thesis is also outlined and the main contributions are described.

1.1 Background

The first industry revolution originated from the UK in the mid-19th century, as the steam-powered energy conversion technology replaced the conventional handcraft in the industrial production. Then, in the first decade of the 20th century, electrical power and electrical communication emerged along with the oil-powered internal combustion engine, giving rise to the second industrial revolution. Since late 20th century, the Internet technology and renewable energy marked the rise of the third industrial revolution. Distributed communication revolution converges with a new distributed energy via smart inter-connections. Three industrial revolutions push the social productivity to an unprecedented high level, but it also brings about many negative influences on the environments due to the lack of rational exploitation and

utilization of fossil fuels and unsustainable energy production and consumption [1].

On the other hand, the limited mineable reserves of fossil fuels and their unbalanced distribution also led to three times of global energy crises during last century. In regarding the response to the crisis, the international community has reached an agreement that it is necessary to reform the existing mode of energy production and consumption, which relies on fossil fuels, to a sustainable mode with clean alternative energy sources and low carbon emissions [2]. On the energy supply side, various renewable generation sources are integrated into the power grid, such as solar energy, tidal energy, and especially wind energy, whose penetration steadily grows [3]; On the energy demand side, electric vehicles are becoming more and more popular due to their advantages such as low exhaust emissions and high energy efficiency. The marketplace of electric vehicles is emerging in both developed and developing countries in recent years [4].

1.1.1 Electric Vehicle Popularization

An electric vehicle is an automobile that is propelled by its electric motor, and equipped with a certain electric energy storage infrastructure onboard [5]. Electric vehicles have advantages in energy efficiency and exhaust emission compared with conventional internal combustion based automobiles [6]-[7].

In recent years, electric vehicles have been drawing great attentions from both the governments and the public in their development and popularization. For example, in the U.S., a series incentive policies have been launched by the government for both

customers and manufactures, so that a mature domestic market can be formulated in around 2015~2017, with potential sales of 1 to 1.5 million plug-in hybrid electric vehicles [8]; As for China, the second largest vehicle market, the government also emphasizes its electric vehicle industry as one of the promising industry, it is committed to establish a public transportation system based on electric vehicles [9]; In late 2008, the European Commission launched the “European Green Cars” project while the European Investment Bank offered an initial budget of €5 billion. Figure 1-1 is the forecast of electric vehicle market in 2020 [10].

Figure 1-1 The Estimated Global Alternative-Energy Vehicle Map in 2020

On the other hand, public infrastructures for large-scale charging should be established in order to offer rapid and convenient services for the consumers to support the popularization of electric vehicles. For example, the ChargePoint America project in the U.S. is aimed at building some 5,000 charging stations to provide charging services [11]; Moreover, the Multi-state Electric Vehicle Project is aimed at

building 15,000 charging points in 16 major cities and metropolitan areas in 6 states [12]. In China, according to the three-step development plan of the State-Grid Corporation, 75 charging stations and 6,209 charging poles had been built during 2009-2010, then 4,000 charging stations are being built in the next 5 years and finally a complete interconnected charging network consisting of 10,000 charging stations will be established by 2020 [13]. European governments have also proposed a series of promotional plans for electric vehicles. For examples, the French government has planned to establish a national wide electric vehicle charging network containing over 4 million charging points by 2020 [14]; in the UK, more than 25,000 charging points will be installed across London as well as other cities by 2015[15].

1.1.2 Wind Generation Development

The popularization of electric vehicles will need to consider an optimization on the power demand side for environment protection and sustainability, while the power supply side is also undergoing a reform, which is represented by the rapid development of wind generation.

Wind energy is considered to be clean, safe and sustainable, which now dominates the position in the new energy area. The origin of wind energy utilization can date back to the 19th century, when windmills were developed to extract the kinetic energy existing in wind flows as mechanical energy. Then the first wind generator was invented sooner and the first wind farm was built in Denmark in the late 19th century. During 1970s-1980s, in order to overcome the energy crisis, great attention was paid

on sustainable energy, during this period, the first 55 kW wind generator was developed, representing a breakthrough in modern wind power industry [16]. From then on, not only the capacity of a wind generator reaches kW and MW levels but also the requirements on reliability and efficiency of a wind generator become essential [17].

In recent years, worldwide installed wind power capacity reached 239 GW by the end of 2011, among which the five leading countries are China, USA, Germany, Spain and India, together representing a total share of 74% of the global wind capacity [18].

UK, as the windiest country in Europe, has been exploiting wind resources since the beginning of the 21th century as shown in [19]:

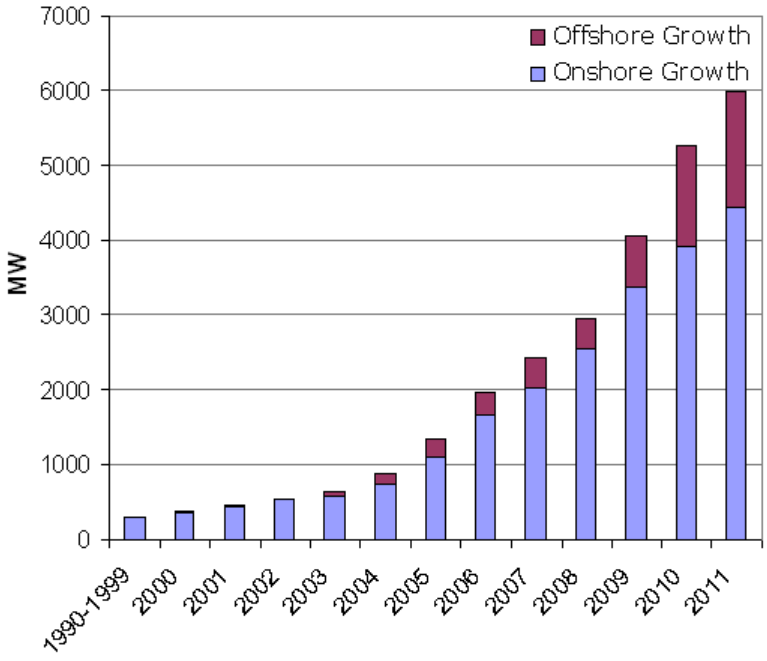

Figure 1-2 UK installed Wind Power Capacity (in MW)

The installed wind power capacity is expected to continue growing in the UK for the

foreseeable future, especially for offshore wind power, because UK has been estimated to have over a third of Europe's total offshore wind energy resource. In fact, UK government plans 13GW of installed offshore wind power capacity by 2020, and had completed 3 rounds of project biddings for offshore wind farms since 1998. Currently, UK has 1.86GW of operational nameplate capacity, with a further 2.05GW under construction [19].

Because of the inherent fluctuation and intermittence of wind energy, the large integration of wind power generation led to a large amount of negative effects on the power system in stability, reliability and power quality [20]. Due to these shortcomings, wind power generation is not as reliable or controllable as the conventional thermal power generation, so extra reserve capacity should be equipped with the wind power generators from the prospective of power system reliability. On the other hand, early wind generators draw reactive power during their operation, which mainly used for voltage regulation in modern wind power generator.

With the popularization of electric vehicles in the transportation system, the electrical energy sector will encounter a dramatic change due to this important and expected issue. The impact of electric vehicles on power systems mainly occurs on the demand side [21]-[22]: The number of electric vehicles directly determines the degree of their impact on power grids. With the rapid growth of electric vehicles in recent years, their overall charging demand will become an important part of system loads.

It has been discovered that a high penetration of electric vehicles will increase

electricity consumption during their charging periods, which could lead to considerable change in the power flows, grid losses, and voltage profile patterns of the power grid.

It is also found that the amount of intermittent renewable energy resources that can be safely integrated into the power system may increase due to the proper utilization of distributed electric vehicle storage capacity [23]. When the primary renewable energy resources are available, electric vehicles can be charged to store energy and inject it into system later when necessary. In this way, the spillage of clean energy in the system could be avoided, so that the usage of the conventional fossil fuel units and expensive generating units could be decreased during peak hours [24]. This will also reduce pollutant emissions and generation costs.

1.2 Literature Review

The electric vehicle is generally made up of a drive train that at least contains an electrical motor, a battery storage system and/or a means of recharging the battery from an external source of electricity [23]. Its battery capacity usually ranges from several kWh or tens of kWh to power the vehicle in all electric drive mode for several tens of miles [24]. Moreover, an electric vehicle may have an internal combustion engine as well, in order to extend its drive range when it runs out of its battery [25].

Research on the impact of electric vehicle charging on the power grid dated back to the 1980s. It was discovered that the charging demand of electric vehicles tends to

coincide with the overall peak load [26]. Therefore, when the penetration of electric vehicles increases, it is necessary to manage their charging demand, in order to avoid significant increase of the overall peak load [27]-[28]. Later, the so-called smart charging was proposed, whose target is to optimize the charging process of electric vehicles [29]-[34]:

A control strategy was proposed in [29] to minimize the energy consumption of electric vehicle charging in a residential use case. Another two strategies were presented in [30] to control the charging time and energy flows of an electric car, considering forecasted electricity price and system auxiliary service. In [30]-[31], the potential benefits of electric vehicles as some type of auxiliary service were discussed, and a conceptual framework for implementation was presented in [32]-[33].

However, though smart charging has demonstrated a good potential in the future smart grid, currently most consumers in reality still prefer to charge their electric vehicles as fast as possible. In this situation, smart charging control should not interfere with their daily drive profile [31]-[34]. On the other hand, the fast developing rapid charging techniques are [35] attracting more electric vehicle consumers. Moreover, the implementation and integration of smart charging in a system wide scale is still a long-time work in future. Therefore, currently it is still necessary to assess the impact of uncontrolled charging of electric vehicles on the power system.

The impact of electric vehicle charging on the power grid can be evaluated by such as

thermal loading, voltage regulation, phase unbalance, power losses, harmonic distortion, and etc. [36]. These are typical metrics for both systemic and component based analysis. Based on this, modeling of power grid components, electric vehicles, and their integration, which reflects the above key physical quantities, becomes important. When electric vehicles are charged, this means increased loading to the distribution grid; when electric vehicles are discharged, this means decreased loading to the system. This two operating scenarios of electric vehicles would have impacts not only on the distribution grid as a whole but also on the system components.

Distribution system power loss was evaluated in [32], where load factor and variation based objective functions were formulated. It has been proved that minimizing the power losses is equivalent to maximizing the load factor while maximizing the load factor is further equivalent to minimizing load variation.

An interesting aspect of electric vehicles is the possibility of integrating the vehicle to grid (V2G) concept into the utility grid. Basically V2G has three key elements: an interface to the distribution grid with energy flow; a control unit built for communication; smart metering used in vehicles [37].

It has been found that the wind profile in New York matches electric vehicles charging characteristics quite well [38]. This conclusion is based on 2 assumptions: electric vehicles can be charged during the periods when power supply is mainly wind power, while the V2G technology is employed to store energy in these vehicles. When the power supply is not adequate, the V2G technology enables the electric

vehicles as distributed generators to stabilize the power grid with less costs and energy losses.

This means that the V2G operation takes place at the moment of high demand while G2V operation happens at the times of low demand. In [39], grid power loss was reduced by minimizing the power transferred from the slack node to the outer-most node in the system during peak load periods. On the other hand, the energy storage from electric vehicles can be used to feed power back to grid via the node, where the electric vehicles are connected. In principle, due to the radial topology of distribution grids, the closer to the root node of the distribution grid, the smaller the impact of the electric vehicle will be on the distribution grid.

1.3 Dissertation Outline

The outline of the dissertation is as follows:

Chapter 2: The equivalent model of electric batteries is developed, in order to evaluate the terminal voltage and power variation during the battery charging and discharging periods.

The concept of electric vehicle fast charging station is summarized and its detailed simulation model is designed to connect the electric vehicle batteries with the distribution network.

Chapter 3: A dynamic model of a wind turbine (WT) of the double fed induction

generator (DFIG) is formulated. Fault ride through ability is tested in this model.

Chapter 4:The active distribution system is proposed. And the interaction between electric vehicle and distributed wind power generator is investigated in the distribution system when a fault applied in the active distribution system.

Chapter 5: Conclusions are drawn.

1.4 Contributions and objectives

1.4.1 Contributions

Detailed models for the conventional Lead-acid battery and lately popularized Li-ion battery used for an electric vehicle are proposed for power system transient analysis.

A simulation model for the fast charging station is designed, and corresponding control strategy is developed. The system dynamic profile is presented when electric vehicles are integrated into the distribution system.

A detailed model for DFIG (Double Fed Induction Generator) WT including fault ride through protection is presented. The fault test is also carried out based on this model.

The interaction of wind power generation and electric vehicle charging/discharging is tested in a proposed active distribution network. The system dynamic characteristics are described when a fault is applied in the system.

1.4.2 Objectives

Work has been down to achieve the goals as following,

Building an appropriate model to reflect the electrical characteristics of distributed energy resources (EVs and wind generators) in simulation software.

Investigating the dynamic impacts on power quality when integrating large scales EV charging stations into distribution networks.

Investigating the reliability of active distribution network with distributed energy resources (DERs).

Chapter 2 Modeling of Electric Vehicle Batteries and Electric Vehicle Fast-Charging Stations in the Distribution Network

Abstract: In this chapter, firstly the concept of fast charging is introduced, and then the simulation model of an electric vehicle fast-charging station is designed. Accurate models of typical electric vehicle onboard batteries are built for power system transient analysis. Case study is carried out at the end of this chapter with the integration of the charging station into the existing distribution system.

2.1 Electric Vehicle Fast-Charging Station Design

2.1.1 The Concept of Electric Vehicle Fast-Charging

Fast-charging means that the battery consumes a higher voltage or higher current in order to get fully charged in a relatively short time (e.g., less than 60 minutes). The progress of fast-charging can be divided into three steps:

Step 1: This phase is called constant-current charging when the battery is charged at a constant current, until its terminal voltage approaches the gassing voltage [40];

Step 2: This phase is called constant-voltage charging, in this period, the battery is charged at a constant voltage, and this charging voltage is equivalent to the gassing voltage mentioned last paragraph. In the first charging period, when

the battery consuming high charging current, its terminal voltage and internal resistance keep increasing. After the first charging phase finishes, the battery voltage is maintained. However, due to the increasing internal resistance of the battery, the charging current is gradually decreased.

Step 3: When the charging current decreases to a particular value (e.g., 0.015C [41]. C is the unit of charging rate, 1C means the battery require 1 hour to get fully charged), the charger will keep this current value until the battery is fully charged.

2.1.2 Fast-Charging Station Design.

According to the battery characteristics and the charging principles [42], an electric vehicle consuming high voltage and large DC current should meet the requirements of fast-charging. The charging circuit of a charging station usually consists of an AC-DC rectifier connecting the charging station with the distribution network, and a DC-DC converter connected in series with the AC-DC converter to obtain the rated DC voltage [43]. In this chapter, an IGBT-based AC/DC rectifier and a common DC/DC buck converter are adopted for certain reasons, which will be discussed later. The structure of the charging circuit is shown in Figure 2-1:

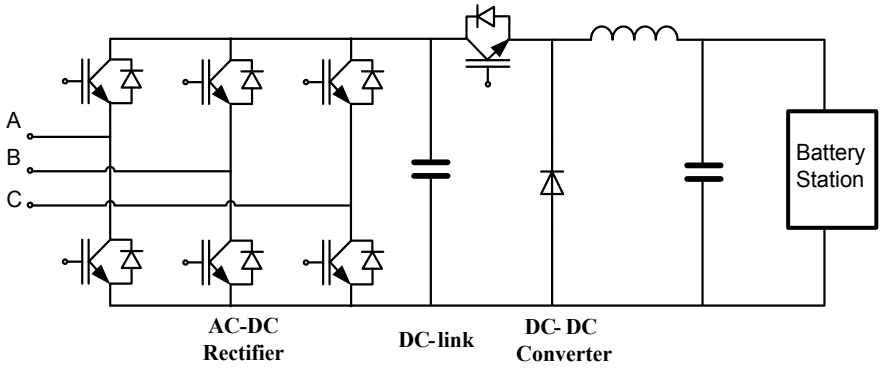

Figure 2-1 The Structure of the Charging Circuit

The AC-DC converter is configured as a two-level, three-phase half-bridge containing 6 pairs of IGBTs and diodes controlled by PWM firing signals. Its controller employs two PI regulators to control the output DC voltage while maintaining a unity input power factor for the AC power supply. The detailed control diagram is shown in Figure 2-2:

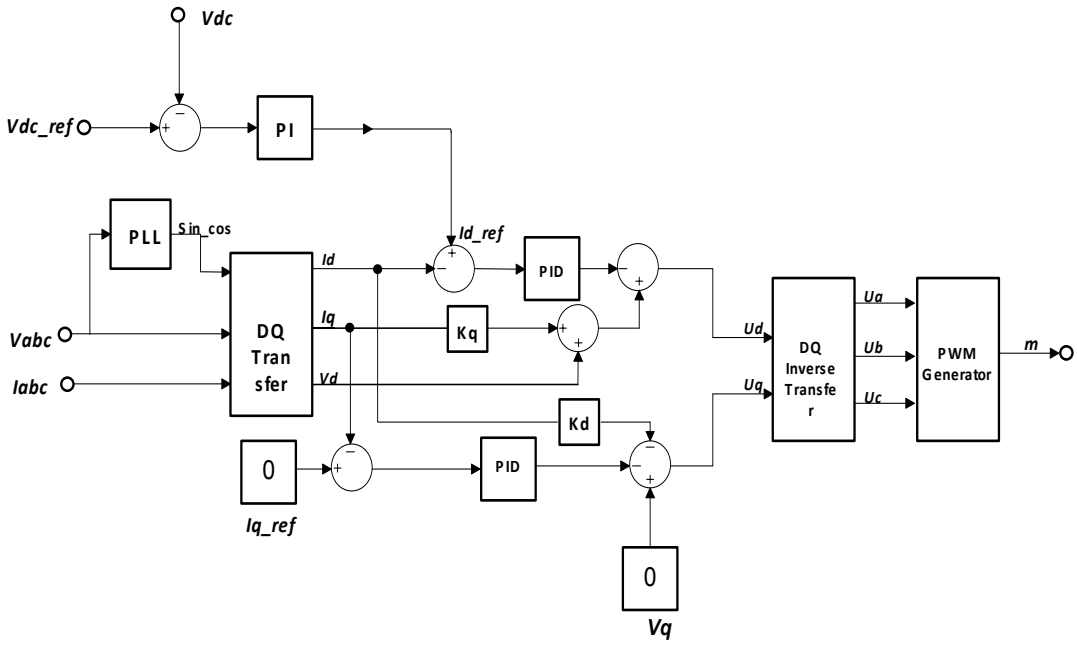

Figure 2-2 The Control Strategy for the AC-DC Rectifier

As shown above, the AC-DC rectifier is modeled in the d-q reference frame. The measured three-phase voltages and currents are transformed into corresponding d-q

frame values. The voltage-oriented control (VOC) strategy is adopted, in which V_q equals to 0. The measured value of the DC voltage is compared with its reference value and then sent to a PI controller as I_d, which is designed for the DC voltage control. On the other hand, the reference of I_q is 0 in order to maintain the unit power factor for input power.

2.2 Modeling of Battery in Power Systems

To estimate the accurate impact on power capacity and determine appropriate components to evaluate these impacts, the battery model is also important to the simulation of electric vehicles, which needs high-fidelity to achieve meaningful simulation results.

2.2.1 Transient Model of Li-ion Battery

The output voltage of the battery can be calculated from its open-circuit voltage, and the voltage drop resulting from its equivalent internal impedance. Accordingly, the battery output voltage can be expressed as

$$V_{bat} = V_{oc} - i_{batt} \times Z_{eq} + \Delta E(T) \tag{2-1}$$

where the temperature T is assumed constant, $\Delta E(T)$, the temperature range is equals to zero, so it can be neglected. The open-circuit voltage of the battery strongly depends on battery SOC (State of Charge), which can be calculated as [44]

$$V_{oc}(soc) = -1.031 \times \exp(-35 \times SOC) + 3.685 + 0.2156 \times SOC - 0.1178 \times SOC^2 + 0.321 \times SOC^3 \tag{2-2}$$

The battery SOC can be expressed as

$$SOC = SOC_{init} - \int (i_{bat} / C_{usable})dt \tag{2-3}$$

The equivalent internal impedance of the battery consists of a series resistor (R_{series}, R_{cycle}) and two RC networks ($R_{Transient\_S}$, $C_{Transient\_S}$, $R_{Transient\_L}$ and $C_{Transient\_L}$), as shown in Figure 2-3 as follows

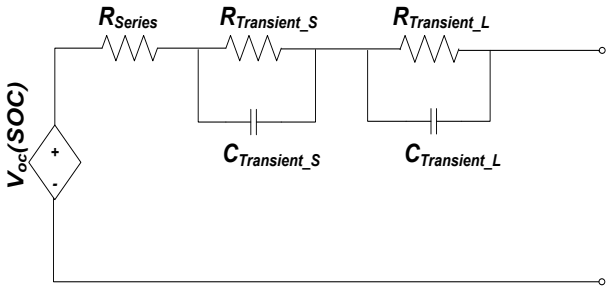

Figure 2-3 The Equivalent Circuit of a Li-Ion Battery

where R_{Series} is responsible for the instantaneous drop in the battery terminal voltage. Note that, R_{cycle} is used to explain the increase in the battery resistance with cycling, which is neglected in this model.

The RC components are responsible for short and long time transients in the battery internal impedance. The values of R_{Series}, $R_{Transient\_S}$, $C_{Transient\_S}$, $R_{Transient\_L}$ and $C_{Transient\_L}$ can be calculated from the battery SOC as following,

$$R_{series}(SOC) = 0.1562 \times \exp(-24.37 \times SOC) + 0.07446 \tag{2-4}$$

$$R_{Transient\_S}(SOC) = 0.3208 \times \exp(-29.14 \times SOC) + 0.04669 \tag{2-5}$$

$$C_{Transient\_S}(SOC) = 752.9 \times \exp(-13.51 \times SOC) + 703.6 \tag{2-6}$$

$$R_{Transient\_L}(SOC) = 6.603 \times \exp(-155.2 \times SOC) + 0.04984 \tag{2-7}$$

The charging profiles of an electric vehicle is represented by the model and

parameters given in [44]-[46]. The equivalent circuit of its Li-ion battery cell is given in Figure 2-3. The nonlinear relationship between the open-circuit voltage V_{oc} and the status of charging (*SOC*) is represented by a controllable voltage source. R_{Series} $R_{Transient\_S}$, $C_{Tansient\_S}$, $R_{Transient\_L}$, and $C_{Transient\_L}$ are all the functions of *SOC*, so that short and long time constants that describe the step response of the battery voltage can be taken into consideration [44].

In an electric vehicle, the required values of terminal voltage and power capacity for the power grid and the energy storage system are obtained by arranging multiple battery cells in series and parallel. The cells that are in series determine the terminal voltage of a battery stack, and the number of parallel cells decides the current carrying capability of a battery stack. The total capacity of a battery stack is given as

$$C_t = C_i \cdot n_s \cdot n_p \tag{2-8}$$

where C_t is the total capacity of the battery stack (Ah); C_i is the capacity of a single cell (Ah); n_s is the number of cells in series; and n_p is the number of cells in parallel. As given in [46], C_i is set to be 0.85Ah. The modeled Li-ion battery stack is scaled up to 5kWh, standing for the one in the Toyota Prius Hymotion PHEV [47]. Each cell is assumed to operate at 3.8V, so 53 cells in series and 29 cells in parallel constitute a capacity of around 5kWh [48]:

$$E = C_i \cdot n_s \cdot n_p \cdot V_t \approx 0.85 * 53 * 29 * 3.5 \approx 5kWh$$

where V_t is the nominal terminal voltage of each cell (with unit of voltage).

As for its implementation, the output signal of the battery stack is generated through a Simulink model.

2.2.2 Case Studies

In this section, it is assumed that there are ten electric vehicles being charged together in a charging station at the same time, so the total capacity of the charging station should be no less than the summation of their rated capacity. Meanwhile, in the realistic situation few consumers would charge an electric vehicle until the whole battery is totally exhausted. Thus, it is assumed that the initial SOC of the battery is 20% of its rated capacity. In the simulation system shown in Figure 2-4, two charging stations (CS1 and CS2) are connected with 400V Buses B3 and B4, respectively. The simulation system is built and tested in Matlab/Simulink.

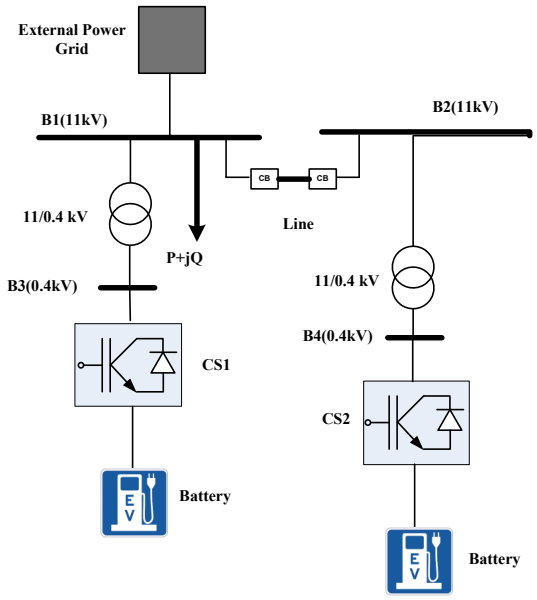

Figure 2-4 The System Layout

Three cases are described as follows:

Case 1: CS1 and CS2 were put into operation at 2.5s simultaneously. The voltage at

the DC-side of the AC-DC rectifier at CS1 is shown in Figure 2-5, where a distinctive voltage dip can be observed. Numerical value refers to the capacity of EV charging station and feeder capacity.

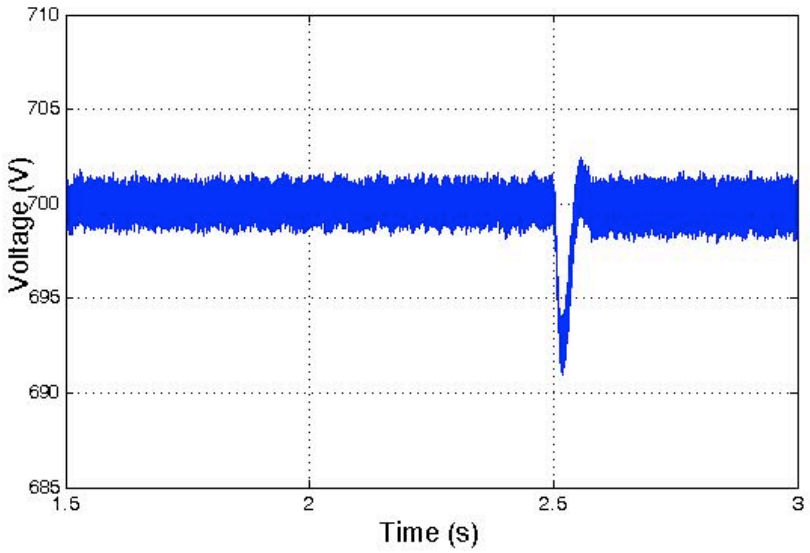

Figure 2-5 The DC voltage on the AC-DC Rectifier of CS1 in Case 1

Figure 2-6 and Figure 2-7 show the dynamic performance of the voltage and current at the coupled connection point (CCP) at CS1. It can be observed at 2.5s, an apparent dip occurred in the DC voltage but then it was stabilized quickly at about 430V.

For the DC current, as the charging stations were put into operation, the CCP acquired a constant current, which means the fast-charging process started from then on.

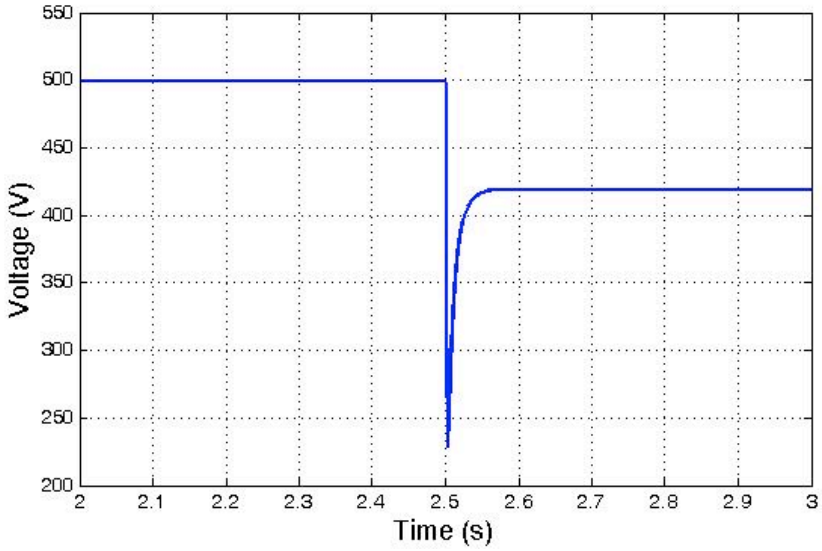

Figure 2-6 The AC Voltage Profile (RMS value) at CS1 in Case 1

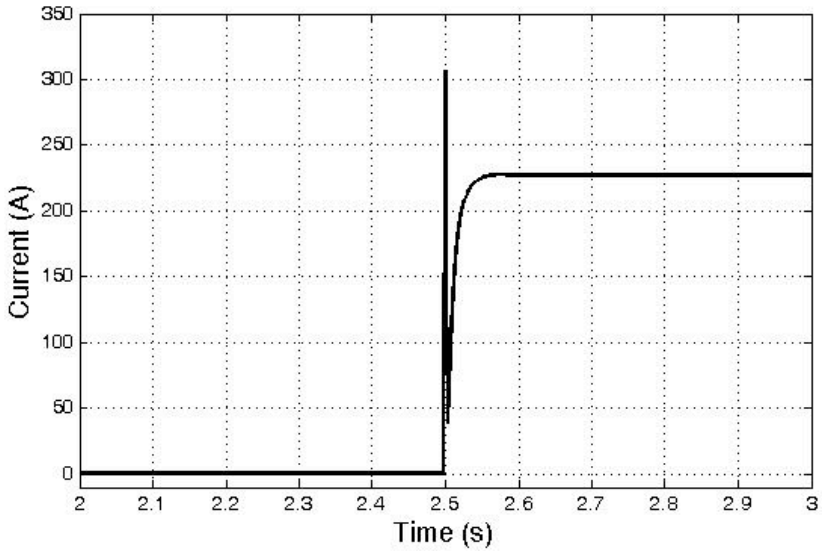

Figure 2-7 The **AC** Current Profile at CS1

Case 2: A permanent 3-phase short-circuit ground fault was applied at Bus B4 at 3.5s. The current at CS2 is shown in Figure 2-9 and the reverse current was shown in the Bus B4. The voltage at CS2 is shown in Figure 2-10.

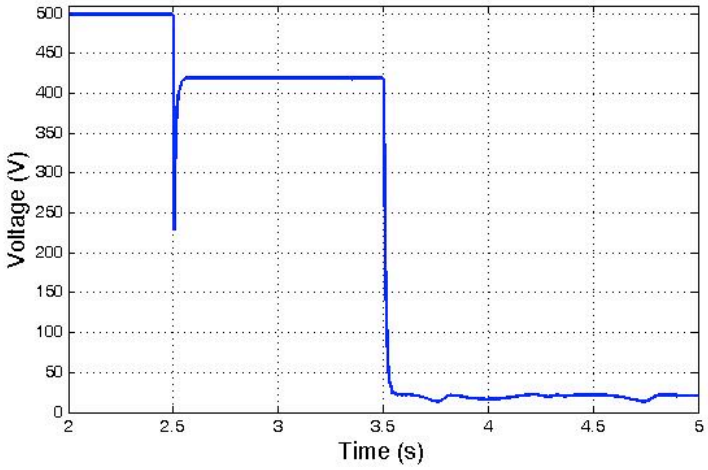

Figure 2-8 The **AC** Voltage Profile at CS2 in Case 2

When the fault was applied, the voltage measured from CS2 decreased to a relatively low value. During the fault, because the battery voltage was higher than the CCP voltage, the charging mode was transferred to the discharge mode. In this situation, the battery became a voltage source injecting power into the distribution network.

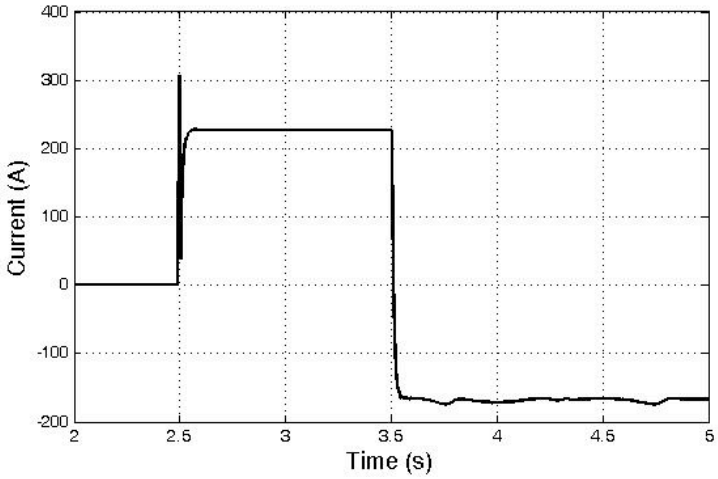

Figure 2-9 The Current Profile at CS2 in Case 2

Case 3: A transient three-phase ground fault was applied at Bus B4 at 3.5s and the fault was cleared at 4.0s. The simulation results of the current and voltage at CS2 are

shown in Figure 2-10 and Figure 2-11 respectively.

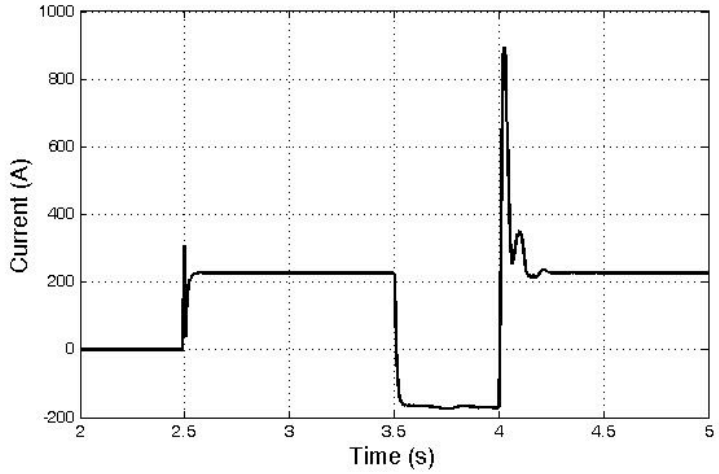

Figure 2-10 The Current Profile at CS2 in Case 3

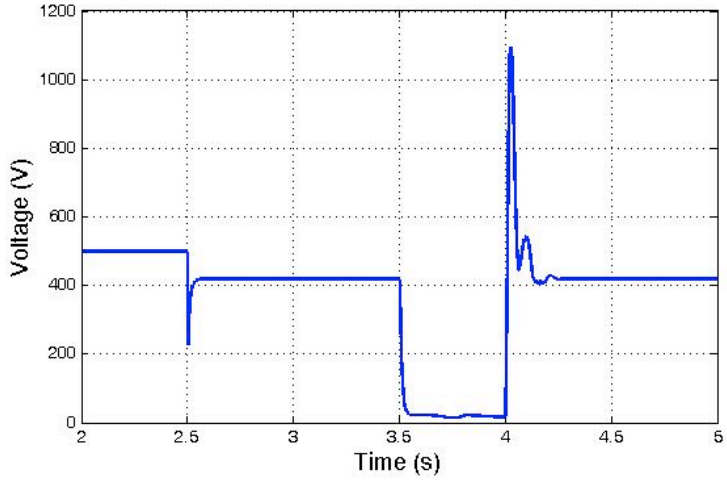

Figure 2-11 The **AC** Voltage Profile at CS2 in Case 3

2.3 Summary

In this chapter, an appropriate model of the electric vehicle fast charging station is designed for the analysis of power system transient stability. Based on the proposed battery model, the dynamic impacts of electric vehicle charging stations on the distribution network have been evaluated in different scenarios.

According to the simulation results, the electric vehicles have the ability to inject power to the utility grid when the grid fault applied, which may help to make the CCP voltage stable and hence improve power system stability.

Chapter 3 Modeling of Wind Power Generation with Fault Ride-through Ability in Electricity Distribution Networks

Abstract: In this chapter, the modeling of a wind turbine with DFIG is reviewed first. Then an introduction to the fault ride-through ability of the wind generator is also made in this chapter. The simulation model of the DFIG with a wind turbine is built in Matlab/Simulink with the fault ride-through ability using the crowbar protection principle. Case study is used to verify that the crowbar fulfills its function to prevent excess rotor current through the rotor side converter.

3.1 Introduction

3.1.1 Review on Modelling of DFIG with Wind Turbine

The Doubly Fed Induction Generator (DFIG) is widely used in wind power generation, in which the induction generator is assembled with a multi-phase wound rotor and a multi-phase slip ring. The rotor winding of the DFIG is connected to the grid via slip rings and a back-to-back voltage source converter (VSC). This converter is designed to control the rotor current and the grid current. With its rotor currents controlled by the converter, the active and reactive power output of such a generator can be adjusted by varying the rotating speed of its stator.

The DFIG has several advantages over the conventional induction generator:

1. The DFIG has the ability to either draw or send reactive power from/to the grid. This brings a great benefit for power system stability by allowing the machine to support the grid operations during severe voltage disturbances (i.e. low voltage ride-through, LVRT).
2. The control of the rotor voltages and currents will enable the induction machine to remain synchronized with the grid while the wind turbine speed varies. It has been recognized that the variable speed wind turbine is more efficient than a fixed speed wind turbine, especially when the wind speed is low.
3. The cost of the power electronic converter is lower than other solutions for the variable speed wind turbine, because only part of the mechanical power (typically 25%-30%) is fed to the grid through the converter, while the rest is fed to the grid directly from the stator.

A DFIG is typically given as a fifth-order dynamic model considering both the electromagnetic transients of the stator and the flux transients of the rotor [48] -[49]. By neglecting the stator electrical dynamics, such a fifth-order dynamic model of DFIG with a wind turbine can be reduced to a third-order one. If the rotor electrical dynamics are further neglected, a reduced first-order dynamic model can be obtained [50].

The dynamic DFIG models of different orders have been compared in [51].The results have indicated that under the torque disturbance, the responses of the fifth-order

model and the third-order model are similar, while that of the first-order model is different.

The validation of the dynamic models of the DFIG has been made in [52] [52]. The comparison has shown that the dynamics of the DFIG can be formulated properly by the fifth-order model. Therefore, such a detailed model has been well widely used in the dynamic simulation of the DFIG and its controllers' design [53].

In principle, if the dynamics of the Wind Turbine (WT) with DFIG is concerned, then the detailed model is preferred, while the third-order model becomes more attractive in the classical electro-mechanical dynamic studies of large power systems [54].

Basically, the DFIG is driven by the drive train of the WT system. Such a driven train is generally composed of a turbine, a gearbox, shafts and some other mechanical components. We assume here that the gearbox and the high speed shaft are infinitely stiff, the drive train can be represented by a two-mass model, including the turbine and the generator [55]. In some cases, the drive train can be lumped together into an equivalent mass model [56]-[57].

For the large-scale wind farm, aggregated models for the wind farm have been proposed to reduce the simulation time. In [58], an equivalent one-machine model was developed to represent the wind farm. It can be used to represent the wind farm only when all the wind turbines are operated under the same or similar condition. Otherwise, the detailed multi-machine model should be employed due to the effects of

irregular wind distribution and geographical distribution of the wind turbines [59].

3.1.2 Wind Generator Fault Ride-through Ability

Wind turbines are required to have the ability to remain connected with the electric grid, when the grid voltage temporarily drops due to a certain fault or change in the grid. This is defined as the so-called low voltage ride through (LVRT) or fault ride through (FRT). The required LVRT behavior is defined in the grid code specified by electricity grid operators. For example, the grid code issued by UK National Grid Company requires that wind turbines should remain transiently stable and connected to the system without tripping any other generators. For any balanced or unbalanced voltage dip on the low voltage side, its voltage profile should be anywhere on or above the black line as shown in Figure 3-1 [60], where V/VN (%) is the ratio of the actual voltage on one or more phases to the nominal voltage on the low voltage side. For avoidance of doubt, the profile beyond 140ms in Figure 3-1 is the minimum recovery in voltage that will be accepted by the generator following the clearance of the fault at 140ms.

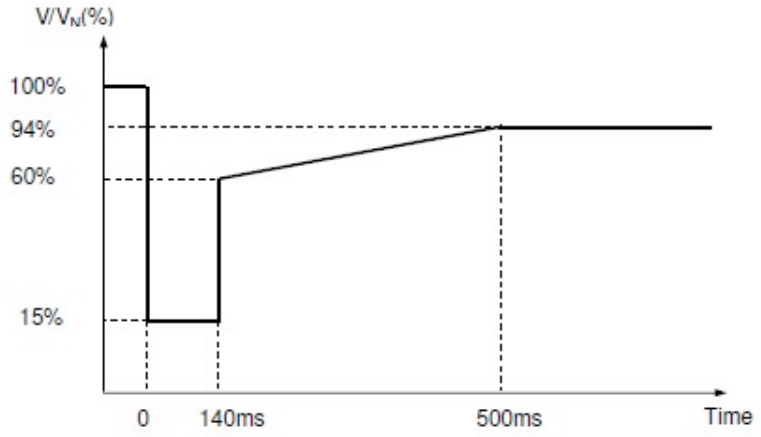

Figure 3-1 Fault Ride through Requirement in UK National Grid's Grid Code

3.2 Modelling Wind Turbine with DFIG

3.2.1 Modelling of DFIG

The stator voltage equations, rotor voltage equations and the flux linkage equations in *d-q* reference frame can be written as follows [61].

Stator voltage equations:

$$u_{ds} = R_s i_{ds} - \omega_s \psi_{qs} + \frac{d\psi_{ds}}{dt} \tag{3-1}$$

$$u_{qs} = R_s i_{qs} + \omega_s \psi_{ds} + \frac{d\psi_{qs}}{dt} \tag{3-2}$$

Rotor voltage equations:

$$u_{dr} = R_r i_{dr} - s_r \omega_s \psi_{qr} + \frac{d\psi_{dr}}{dt} \tag{3-3}$$

$$u_{qr} = R_r i_{qr} - s_r \omega_s \psi_{dr} + \frac{d\psi_{qr}}{dt} \tag{3-4}$$

Flux linkage equations:

$$\psi_{ds} = L_{ss} i_{ds} + L_m i_{dr} \tag{3-5}$$

$$\psi_{qs} = L_{ss} i_{qs} + L_m i_{qr} \tag{3-6}$$

$$\psi_{dr} = L_{rr} i_{dr} + L_m i_{ds} \tag{3-7}$$

$$\psi_{qr} = L_{rr} i_{qr} + L_m i_{qs} \tag{3-8}$$

The equivalent circuits for the DFIG with direct axis (d-axis) and quadrature axis (q-axis) are also described in Figure 3-2:

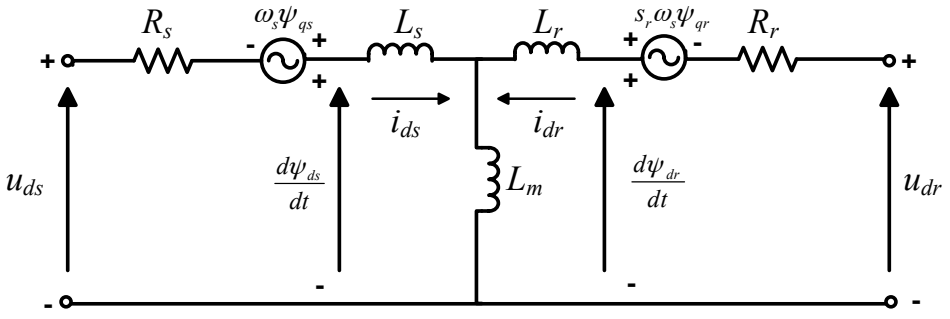

(a) d-axis equivalent circuit

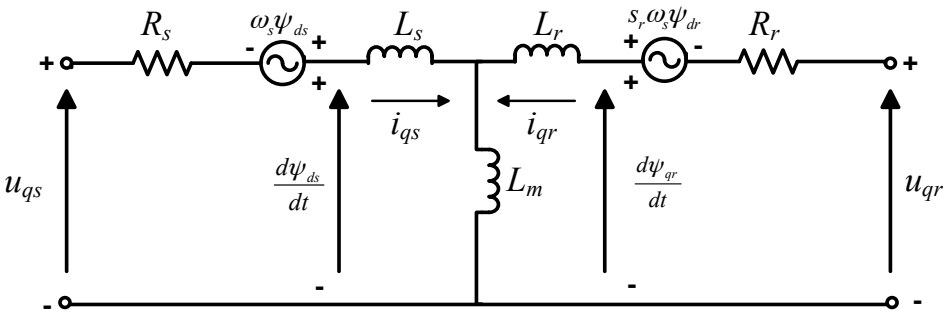

(b) *q*-axis equivalent circuit

Figure 3-2 The Equivalent Circuits for the DFIG

where,

ψ_{ds}	direct (*d*) axis stator flux linkages;

ψ_{qs}	quadrature (q) axis stator flux linkages;
ψ_{dr}	direct (d) axis rotor flux linkage;
ψ_{qr}	quadrature (q) axis rotor flux linkage;
L_m	mutual inductance;
L_{ss}	stator self-inductance, $L_{ss}=L_s+L_m$;
L_{rr}	rotor self-inductance, and $L_{rr}=L_r+L_{m;}$
Rr	rotor resistance;
ω_s	synchronous angular speed;
s_r	rotor slip;
i_{ds}	d axis stator currents;
i_{qs}	q axis stator currents;
v_{ds}	d axis stator terminal voltages;
v_{qs}	q axis stator terminal voltages;
v_{dr}	d axis rotor voltages,
v_{qr}	q axis rotor voltages,

If we define $E'_d = -\frac{\omega_s L_m}{L_{rr}}\psi_{qr}$, $E'_q = \frac{\omega_s L_m}{L_{rr}}\psi_{dr}$, $X_s = \omega_s L_{ss}$, $X'_s = \omega_s(L_{ss} - \frac{L_m^{\,2}}{L_{rr}})$, and $T'_0 = \frac{L_{rr}}{R_r}$, then equations for the DFIG are given by:

$$\frac{dE'_d}{dt} = s_r\omega_s E'_q - \omega_s \frac{L_m}{L_{rr}}u_{qr} - \frac{1}{T'_0}[E'_d + (X_s - X'_s)i_{qs}] \tag{3-9}$$

$$\frac{dE'_q}{dt} = -s_r \omega_s E'_d + \omega_s \frac{L_m}{L_{rr}} u_{dr} - \frac{1}{T'_0}[E'_q - (X_s - X'_s) i_{ds}] \tag{3-10}$$

$$\frac{X'_s}{\omega_s}\frac{di_{ds}}{dt} = u_{ds} - [R_s + \frac{1}{\omega_s T'_0}(X_s - X'_s)] i_{ds} - (1 - s_r) E'_d - \frac{L_m}{L_{rr}} u_{dr} + \frac{1}{\omega_s T'_0} E'_q + X'_s i_{qs} \tag{3-11}$$

$$\frac{X'_s}{\omega_s}\frac{di_{qs}}{dt} = u_{qs} - [R_s + \frac{1}{\omega_s T'_0}(X_s - X'_s)] i_{qs} - (1 - s_r) E'_q - \frac{L_m}{L_{rr}} u_{qr} - \frac{1}{\omega_s T'_0} E'_d - X'_s i_{ds} \tag{3-12}$$

where,

E'_d	*d* axis voltages behind the transient reactance;
E'_q	*q* axis voltages behind the transient reactance;
X_s	stator reactance;
X'_s	stator transient reactance;
T'_0	rotor circuit time constant.

3.2.2 Modeling of Drive Train

The drive train, usually represented by a two-mass model, is made up of a turbine, a gearbox, some shafts and other mechanical components. The rotor shaft is flexibly connected to the turbine shaft through the gearbox and coupling. The configuration of the drive train is shown in Figure 3-3:

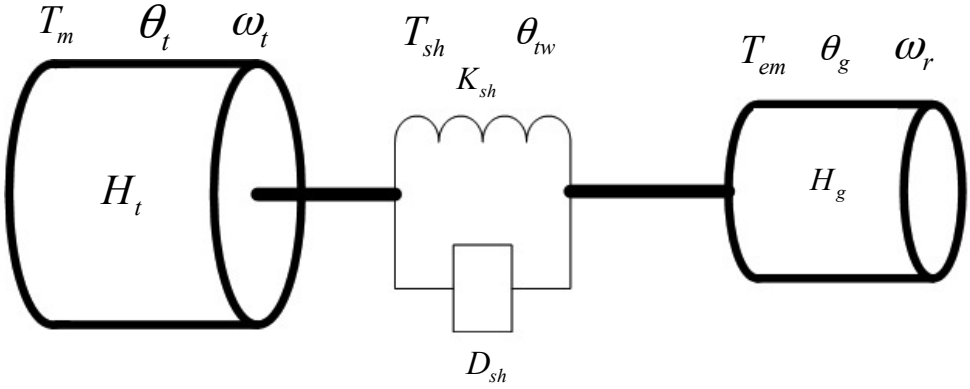

Figure 3-3 Configuration of the Drive Train

and the two-mass model is given by

$$2H_t \frac{d\omega_t}{dt} = T_m - T_{sh} \tag{3-13}$$

$$\frac{d\theta_{tw}}{dt} = \omega_t - \omega_r = \omega_t - (1 - s_r)\omega_s \tag{3-14}$$

$$2H_g \omega_s \frac{ds_r}{dt} = -T_{em} - T_{sh} \tag{3-15}$$

$$\theta_{tw} = \theta_t - \theta_g \tag{3-16}$$

$$T_{sh} = K_{sh}\theta_{tw} + D_{sh}\frac{d\theta_{tw}}{dt} \tag{3-17}$$

where

H_t	inertia constant of the turbine;
H_g	inertia constant of the generator;
ω_t	wind turbine angular speed;
ω_r	generator rotor angular speed;
s_r	rotor slip $s_r = (\omega_s - \omega_r)/\omega_s$;
θ_{tw}	shaft twist angle;
θ_t	turbine rotor angle;

θ_g	generator rotor angle;
K_{sh}	shaft stiffness coefficient;
D_{sh}	damping coefficient;
T_{sh}	shaft torque;
T_{em}	electromagnetic torque of DFIG;
T_m	wind turbine mechanical torque;

If neglecting the power loss in the stator, T_{em} is given by

$$T_{em} = P_s / \omega_s \tag{3-18}$$

T_m is given by

$$T_m = \frac{0.5\rho\pi R_w^2 C_p V_w^3}{\omega_t} \tag{3-19}$$

where

ρ	air density;
R_w	wind turbine blade radius;
V_w	wind speed;
C_f	blade design constant coefficient;
β	blade pitch angle;
λ	blade tip speed ratio, $\lambda = \omega_t R / V_w$;
C_p	power coefficient,
P_s	stator active power.

3.2.3 Modeling of Back-to-Back Converters

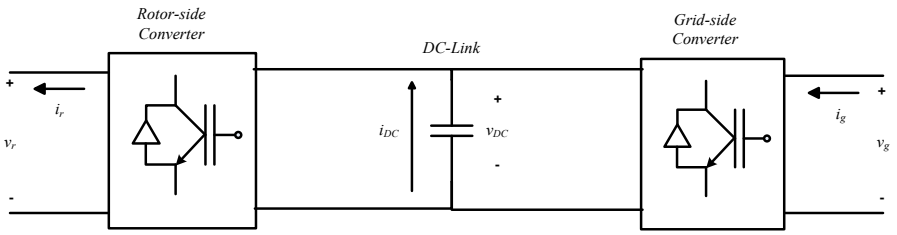

Figure 3-4 The Back-to-back Converter of DFIG

As shown in Figure 3-4, the power balance equation can be expressed as follows,

$$P_r = P_g + P_{DC}. \tag{3-20}$$

$$P_r = v_{dr} i_{dr} + v_{qr} i_{qr} \tag{3-21}$$

$$P_g = v_{dg} i_{dg} + v_{qg} i_{qg} \tag{3-22}$$

$$P_{DC} = v_{DC} i_{DC} = -C v_{DC} \frac{dv_{DC}}{dt} \tag{3-23}$$

where,

P_r	active power at the AC terminal of the rotor side converter;
P_{DC}	instantaneous active power;
i_{dr}	q axis rotor currents of the grid side converter;
i_{dg}	q axis currents of the grid side converter;
v_{dg}	q axis voltages of the grid side converter;
v_{DC}	capacitor DC voltage;
P_g	active power at the AC terminal of the grid side converter;
C	capacitance of the capacitor;
i_{qr}	q axis rotor currents of the grid side converter;
i_{qg}	q axis currents of the grid side converter;

i_{DC}	current of the capacitor;

The power balance equation can be rewritten as

$$Cv_{DC}\frac{dv_{DC}}{dt} = v_{dg}i_{dg} + v_{qg}i_{qg} - (v_{dr}i_{dr} + v_{qr}i_{qr}) \tag{3-24}$$

3.2.4 Modelling of Converter Controller on Rotor Side

The active power and reactive power of DFIG wind generator system is controlled using decoupled control strategies, as proposed in [62].

On the grid side, the active and reactive power outputs are controlled by i_{dg} and i_{qg} respectively, where i_{dg} and i_{qg} can be obtained by aligning the *d* axis of the *d-q* reference frame. Thus, v_{qs} is set to be 0, while v_{ds} equals to the magnitude of the terminal voltage.

On the rotor side, the converter aims to control the active power output of the DFIG by tracking the wind turbine torque, and maintains the required terminal voltage. By aligning the *d* axis of the *d-q* reference with the stator voltage, the active power and terminal voltage are independently controlled by i_{dr} and i_{qr}, respectively. The control diagram is shown in Figure 3-5:

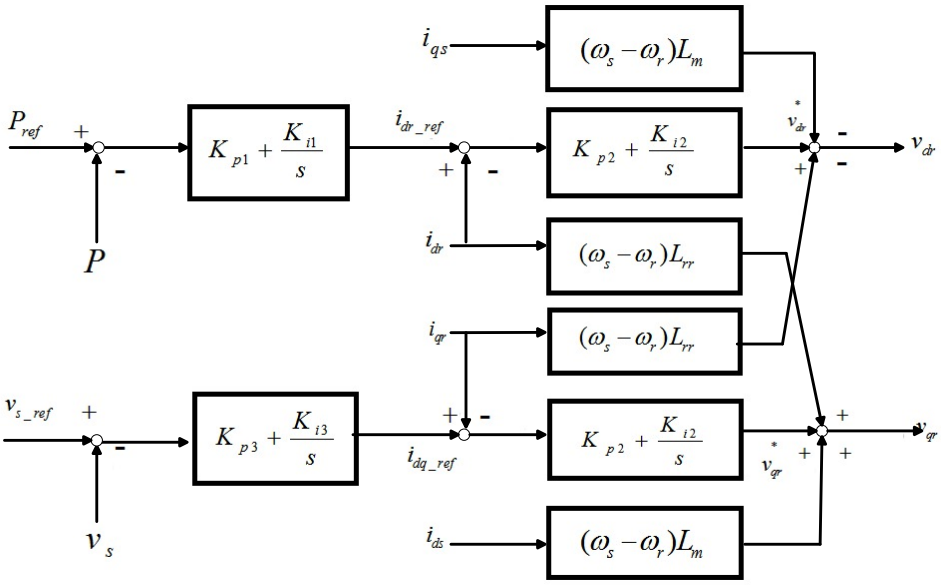

Figure 3-5 Control Block Diagram of the Rotor Side Converter

As shown in Figure. 3-5, this standard DFIG controller consists of two groups of PI-controllers. One group controls the active power by tracking the input wind power, while the other group controls the terminal voltage.

K_{p1}	proportional gains of the power regulator
K_{p2}	proportional gains of the rotor-side converter current regulator
K_{p3}	proportional gains of the grid voltage regulator
i_{dr_ref}	current control references for *d* reference frame of the generator side converter
v_{s_ref}	specified terminal voltage reference
K_{i1}	integrating gains of the power regulator
K_{i2}	integrating gains of the rotor-side converter current regulator
K_{i3}	integrating gains of the grid voltage regulator

i_{qr_ref}	current control references for q reference frame of the generator side converter

P_{ref} is the control reference of the active power of DFIG and is given by

$$P_{ref} = P_B(\frac{\omega_t}{\omega_{tB}})^3 \tag{3-25}$$

where ω_{tB} is the base of the turbine rotating speed; P_B is the maximum active power output at $\omega_t = \omega_{tB}$.

3.2.5 Modelling of Grid Side Converter Controller

As shown in Figure 3-6, the grid side converter controller is responsible for maintaining the DC link voltage, and controlling the terminal reactive power.

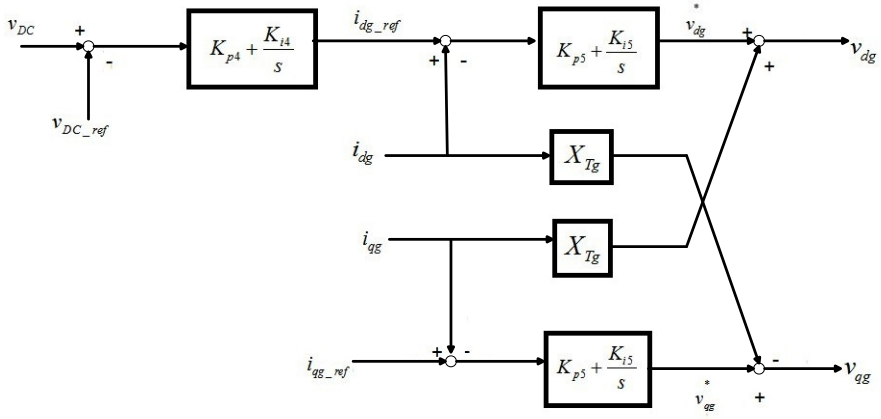

Figure 3-6 Control Block Diagram of Grid Side Converter of DFIG

It consists of two groups of PI controllers as well. One group is for maintaining the DC-Link voltage through i_{dg}, while the other group is for controlling the reactive

power through i_{qg},

K_{p4}	proportional gains of the DC bus voltage regulator
K_{p5}	proportional gains of the grid-side converter current regulator
u_{DC_ref}	voltage control reference of the DC Link
X_{Tg}	the reactance of the fed back transformer
K_{i4}	integrating gains of the DC bus voltage regulator
K_{i5}	integrating gains of the grid-side converter current regulator
i_{qg_ref}	control reference for the q axis component of the grid side converter current

3.2.6 Pitch Controller

The control block diagram of the pitch control is illustrated in Figure 3-7:

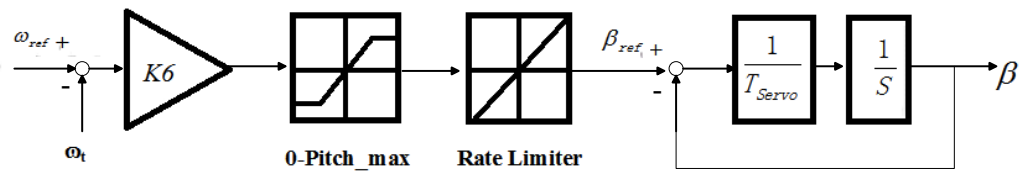

Figure 3-7 Blade Pitch Control for WT with DFIG

In the controller, ω_{ref} is the angular speed of the turbine corresponding to the rated output active power. K_6 is the pitch angle gain; Pitch_max is the maximum value of the pitch angle, and is set to $45°$; the maximum rate of change of the pitch angle is set

to 2 deg/s.

It can be seen in Figure 3-7 that when the rotating speed of the turbine is lower than the rated rotating speed, the pitch angle of the blade is kept at 0 deg. Only when the rotating speed of the turbine is larger than the rated rotating speed, the pitch angle controller is activated to increase the pitch angle. With the increased pitch angle, the power extracted from the wind is decreased, and the rotating speed of the turbine can be maintained at the rated rotating speed.

3.2.7 Integration with Power Grid

The network voltage equation and the wind turbine model are presented in *x-y* and *d-q* reference frames, respectively. Figure 3-8 illustrates the relationship between these two reference frames, where φ is the angle difference between the reference bus voltage of the power grid and the terminal voltage of the WT, while the corresponding transformation is given by (3-26). By using this relationship, the DFIG model can be interfaced with the power grid equations.

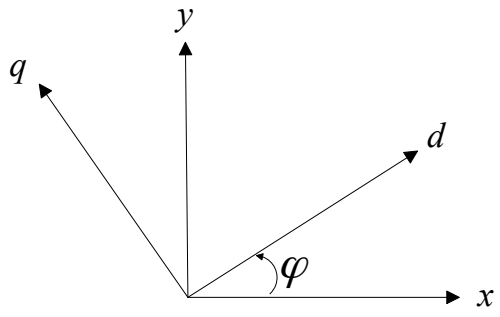

Figure 3-8 The Relationship between *d-q* and *x-y* Frame of Reference

$$\begin{bmatrix} f_d \\ f_q \end{bmatrix} = \begin{bmatrix} \cos\varphi & \sin\varphi \\ -\sin\varphi & \cos\varphi \end{bmatrix} \begin{bmatrix} f_x \\ f_y \end{bmatrix} \tag{3-26}$$

where f_d and f_q are the *d* and *q* reference frame, respectively; f_x and f_y are the *x* and *y* reference frame, respectively.

3.3 Wind Turbine Simulations in MATLAB/SIMULINK

Basically a wind turbine with the DFIG contains a wound rotor induction generator and an AC/DC/AC IGBT-based PWM converter. The stator winding is connected directly to the grid while the rotor is fed at a variable frequency through the back to back AC/DC/AC converter. The DFIG is allowed to extract the maximum energy from the wind at low wind speeds by optimizing the turbine speed, while minimizing mechanical stresses on the turbine in gusts of wind.

3.3.1Wind Turbine Model

The wind turbine is pitch controlled, and the control signal for its pitch angle β is provide by the DFIG control block. β is adjusted to prevent the generator from over-speed operation. The wind speed is considered to be constant in the simulation model.

3.3.2 Induction Machine Model

The developed induction generator model is a full order model with the derivation of the stator fluxes, which can be used in the accurate transient simulation of power systems. It should be mentioned that saturation is not considered in the model because this only leads to small negligible error. This is due to the fact that the saturate inductance is small enough so that the leakage flux goes through the air [63].

3.3.3 Grid Side Converter

The grid side converter (GSC) is modeled as a universal bridge, in which IGBTs are connected to the IG (Induction Generator) terminals through RL filter. The GSC is controlled to maintain the voltage of the DC-link capacitor constant. In this simulation, the GSC model is designed as unidirectional, so power could only transfer from the IG to the power grid. In this situation, GSC does not contribute to voltage regulation or reactive power injection.

3.3.4 Rotor Side Converter

The rotor side converter (RSC) is modeled as a universal bridge, in which IGBTs are connected to the IG rotor windings. The RSC can control the active power output of the DFIG through the torque reference. This torque reference along with an estimated flux determines the rotor current reference. The RSC model is designed to support the grid voltage by injecting the reactive power into the power grid. A PI controller determines the reference value of the reactive power by comparing the measured the grid voltage and the constant voltage reference.

3.3.5 Crowbar Protection System

The crowbar protection system is considered in the simulation model in order to protect the wind turbine against over-current when a fault is applied in the system. The crowbar is made up of a symmetric three phase Wye-connected resistor

connected to the rotor through a circuit breaker. The breaker is normally opened, unless there is any short-circuit current flows from the crowbar resistance into the rotor, or either the rotor current or the DC-link capacitor voltage becomes abnormal. The value of the crowbar resistance is very important since it determines the reactive power drawn by the DFIG while the crowbar is inserted. Generally, the crowbar resistance is selected as 20 times as large as the rotor resistance [64].

3.4 Numerical Examples

3.4.1 Test System Description

The test system used for the case study is shown in Figure 3-9. The wind farm is connected to a 25kV electricity network through a 25kV/0.575kV transformer. The rated capacity of the transformer is 12MVA and the ratio of its rated impedance is 5%. Load is connected at the outlet position of the wind farm. A high-pass capacitor filter is at the wind farm to absorb current harmonics generated by the converters. The wind farm is connected to the 120kV network through a 30km, 25kV transmission line through a 120kV/25kV transformer.

In this case study, the wind farm aggregates 6 units of 1.5 MW DFIG wind turbines, as shown in Figure 3-9. A system ground fault was applied at Bus 25, i.e. the connection point where the wind turbines were connected with the grid via the transmission line. Three phase ground fault was triggered at t = 500ms and cleared at t = 650ms.

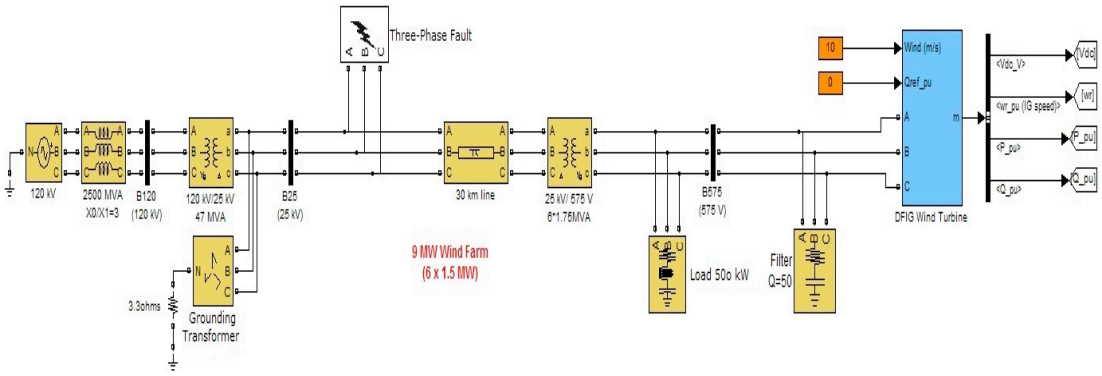

Figure 3-9 Electricity Network Diagram

3.4.2 Simulation Results

The simulation of the wind farm has been done using the described crowbar protection.

Before the fault occurred, the wind farm in steady state feeding 50% of its rated power and drawing no reactive power from the gird. As shown in Figure 3-10, once the fault occurred, the connection point voltage value is below the critical value (generally 0.2pu), crowbar protection of the wind turbines was triggered while RSC stopped switching. Therefore, the rotor current in the crowbar and the rotor windings decayed.

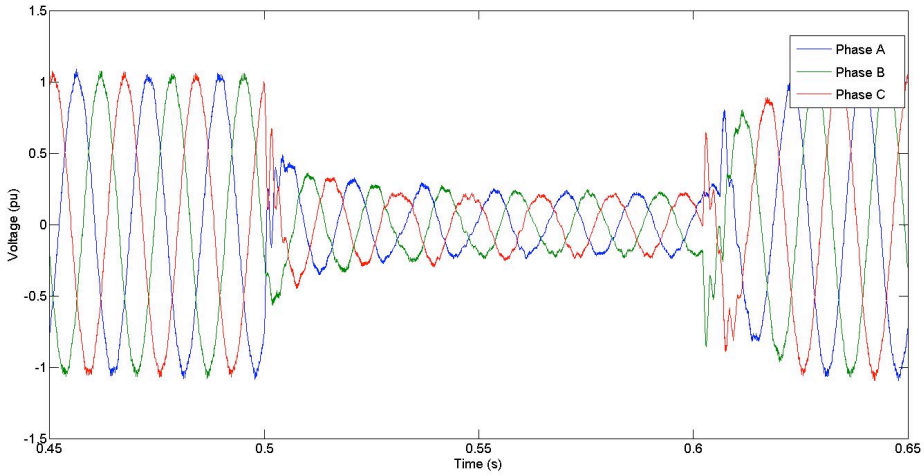

Figure 3-10 Voltage Profile at Bus 575

The DC-link capacitor voltage (shown in Figure 3-11) didn't distinctly increase after the fault happened. But the DC-link voltage increased slightly while the crowbar was connected. It increased dramatically when the fault cleared at t = 650ms. This is because the DFIG absorbed reactive power from the grid after the fault was cleared.

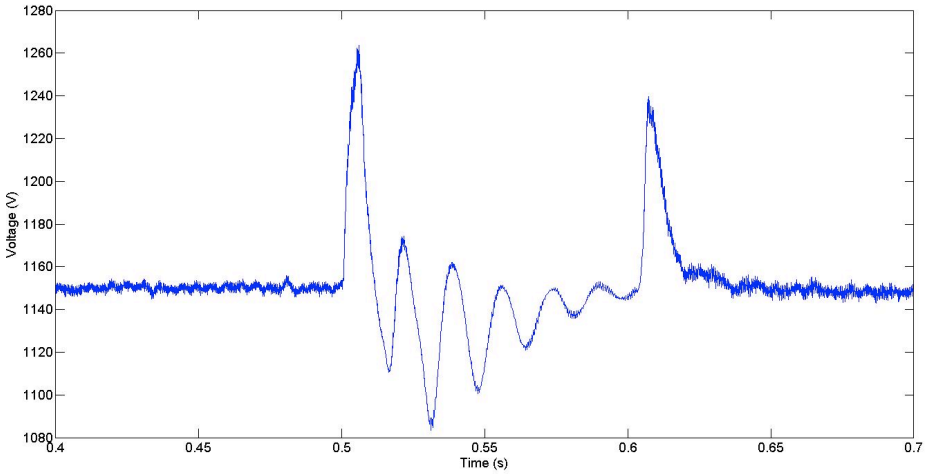

Figure 3-11 Voltage Profile of the DC-link

The RSC started switching again after the fault was cleared, so that the DFIG fed reactive power into the electricity network. The rotor current in the DFIG windings

decreased. The RSC current was equal to 0 when the crowbar triggered. The RSC voltage was higher than the crowbar voltage.

When the fault was cleared, due to the crowbar was still connected due to the high DC-link voltage. The DFIG absorb reactive power, which increased the voltage in the electricity network. The DFIG drew a large amount of reactive power back to the grid, shown in Figure 3-12.

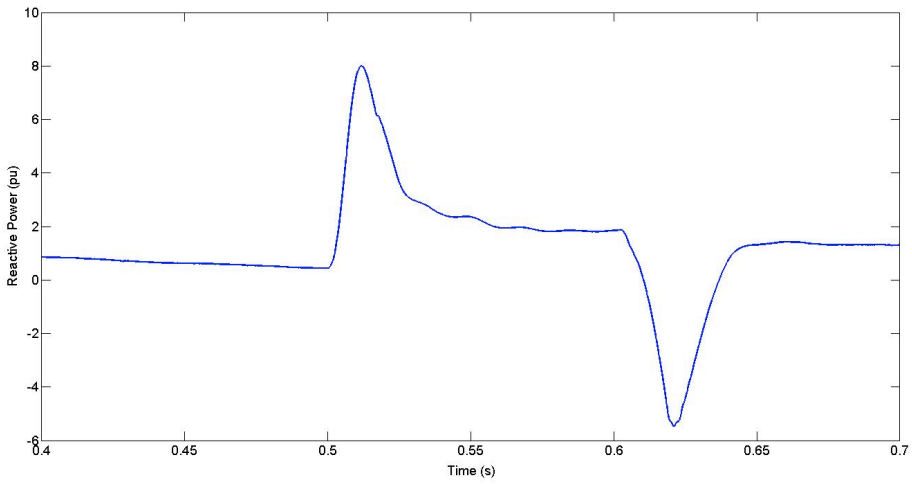

Figure 3-12 Reactive Power Profile of the Wind Farm

3.4 Summary

In this chapter, the modeling of a wind turbine with DFIG has been presented. As a wind generator requires the fault ride-through ability, crowbar protection was considered in the simulation model. As the simulation results have shown that the crowbar protection makes the DFIG wind turbine ride through faults, if the DC-link capacitor voltage is within an acceptable range. The crowbar dissipates the excessive active power and prevents the DC-link capacitor voltage from unnecessary increase,

which may lead to a higher rotor current through the RSC.

Chapter 4 The Interaction between Fast-Charging Stations and Wind Turbines in Distribution Networks

4.1 Introduction

The vehicle-to-grid (V2G) concept means that the electric vehicles can act as both distributed energy storage units and voltage source in power system with a high penetration [65]. The V2G system has the ability to transfer energy between their onboard batteries and the power grid when electric vehicles are plugged into charging poles. The reliability of the power system with renewable energy can be enhanced by V2G if enough electric vehicles are connected with the grid, because electric vehicles can be considered as extra energy reserve storage [66].

In the transmission systems, wind generators are required to have the ability of low voltage ride-through, which makes it remain connected with the grid even when the grid voltage is temporarily dropped due to some faults. In the UK, the grid code issued by the UK National Grid Company [69] is shown in Figure 3-1.

However, when the wind generator has to operate in some extreme conditions, e.g. the grid is experiencing some extreme fault, the voltage at the connection point of the wind generator might fall below the critical value. Under the circumstances, the wind generator will be disconnected from the grid. If a large number of wind generators are

disconnected from the grid, it will cause a severe disturbance in the grid, i.e. sudden loss of wind turbines, which will further cause the fluctuation of voltage and frequency, and threaten the stability of the power system.

In this chapter, the research aims at verifying that the electric vehicles have the potential ability to improve wind generator operational reliability by transferring energy between electric vehicle battery pack and the utility grid. Case study will be carried out by monitoring the system voltage when a fault happens in distribution networks. According to the concept of V2G, electric vehicles are considered as distributed energy resources and charging stations are designed to have the ability of bi-directional power transfer.

4.2 Bidirectional Power Transfer between Electric Vehicle and Distribution Grid

In chapter 2, the electric vehicle battery has been verified with the ability to inject power to the grid when necessary. In this case, the electric vehicle is working in discharging mode.

4.2.1 Interaction between Distribution Grid and Charging Station

The structure of the proposed electric vehicle charging station is made up of a full-bridge inverter/rectifier and a DC-DC converter shown in Figure 4-1. The positive current direction is assumed to be from the grid to the inverter as shown in Figure 4-2.So is the positive power flow direction.

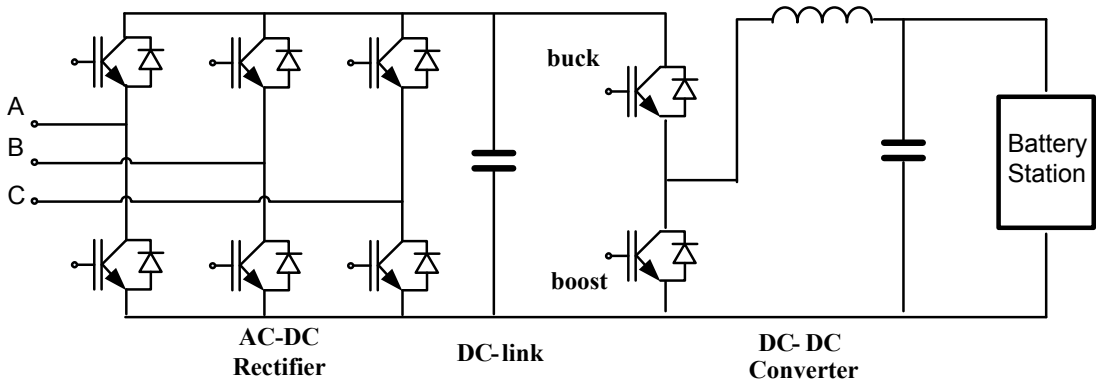

Figure 4-1 Charging Station Structure

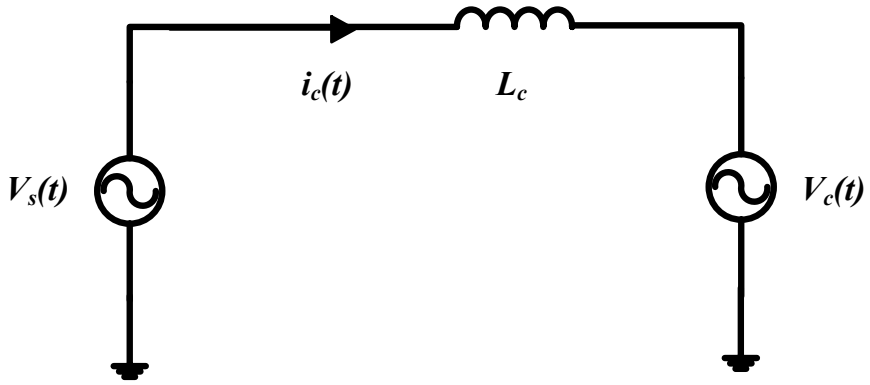

Figure 4-2 The Interaction between the Grid and the Inverter

The system parameters are given as follows:

$v_c(t)$	Instantaneous charging station voltage [V];
$v_s(t)$	Instantaneous grid voltage [V];
$i_c(t)$	Instantaneous charging station current [A];
δ	Phase difference between $v_c(t)$ and $v_s(t)$;
θ	Phase difference between $i_c(t)$ and $v_s(t)$.

Assuming that the grid voltage is purely sinusoidal, high frequency components are neglected. $v_c(t)$ is the inverter output voltage given by the following equations:

$$v_s(t) = \sqrt{2}V_s \sin(\omega t) \tag{4-1}$$

$$v_c(t) = \sqrt{2} \sin(\omega t - \delta) \tag{4-2}$$

A coupling inductor is used and the two voltage sources are decoupled to ensure power transfer from the charging station to the grid. The instantaneous line current of the charging station can be expressed as:

$$i_c(t) = \sqrt{2}I_c \sin(\omega t - \theta) \tag{4-3}$$

Since the default direction for active and reactive power transfer is from the grid to the charging station, $v_c(t)$ lags behind $v_s(t)$ when the charging station operates in charging mode; while $v_s(t)$ lags behind $v_c(t)$ when the charging station operates in discharging mode. The positive direction of active power flow is also defined as from the grid to the charging station. The positive direction of reactive power flow is determined by the phase angle θ. If θ is positive, reactive power is sent to the grid, while if θ is negative, reactive power is drawn from the grid and flows to the charging station. The relationship between these variables is derived as follows

Control variable	P	Q
$v_c(t)$ and δ	$\frac{V_s \times V_c}{X_c} \sin(\delta)$	$\frac{V_s^2}{X_c}[1 - \frac{V_c}{V_s} \cos(\delta)]$
$i_c(t)$ and θ	$V_s \times I_c \times \cos(\theta)$	$V_s \times I_c \times \sin(\theta)$

4.2.2 Control Strategy of Electric Vehicle Charging Station

A. Control of Bidirectional AC-DC inverter

As shown in Figure 4-3, the AC-DC inverter has been modeled in *d-q* reference frame. The three phase voltages and currents in *abc* frame of reference can be transformed into those in *d-q* frame of reference. The voltage-oriented control (VOC) strategy [67] based on dual PI closed-loop has been adopted. The outer loop controller is designed to stabilize DC-link voltage, output current i^*_{gd} on *d*-axis, while the inner loop controller is for DC side current control, by tracking i^*_{gd}.

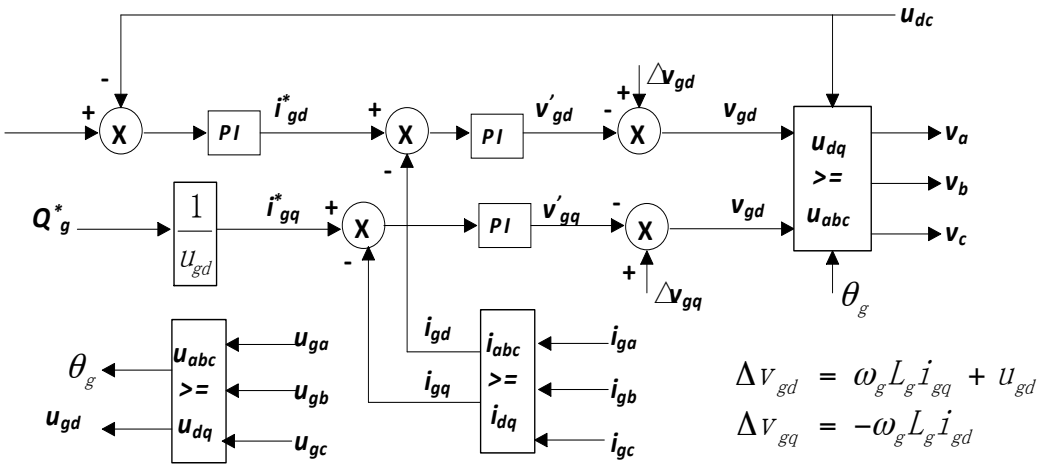

Figure 4-3 Control System Diagram.

It can be found that the cross coupling voltage $\omega_g L_g i_{gq}$ and $-\omega L_g i_{gd}$ are considered in the *d* and *q* axis voltage V_{gd} and V_{gq}, respectively. *d*-axis current is responsible for the DC-link voltage control, of which the reference i^*_{gd} comes from the DC-link voltage control loop; and *q*-axis current is responsible for the control of reactive power Q^*_g.

B. Control of Bidirectional Buck–Boost DC-DC Converter

By changing the duty cycle of the DC-DC converter, both the charging current and charging voltage can be controlled accordingly. The duty cycle reference *d** can be

obtained by designing the closed-loop control strategies as follows.

For charging control, the duty cycle reference d^* can be given by:

$$d^* = u_2 / u_1 + k_p(i_2^* - i_2) + k_i \int (i_2^* - i_2)dt \tag{4-4}$$

For discharging control, the duty cycle reference d^* can be given by:

$$d^* = (u_1 - u_2) / u_1 + k_p(i_2^* - i_2) + k_i \int (i_2^* - i_2)dt \tag{4-5}$$

In (4-4) and (4-5), i_2^* is the reference charging/or discharging current.

4.3 Introduction of Active Distribution Network

The conventional distribution network is a passive network with unidirectional power flow. With the development of distribution energy resources (DERs) such as wind, solar and biomass energy, more and more distributed generation (DG) systems such as wind power generators and PV panels are integrated into the distribution network. With the increasing integration of DG, the infrastructure of the distribution network have been changed from passive to active with the power injection of DERs so the power flow also have been changed from unidirectional to bi-directional in the distribution network. Such a change has brought challenges to the planning, operation, control and protection of the active distribution network involving islanding of DGs, dynamic impacts and so on [64].

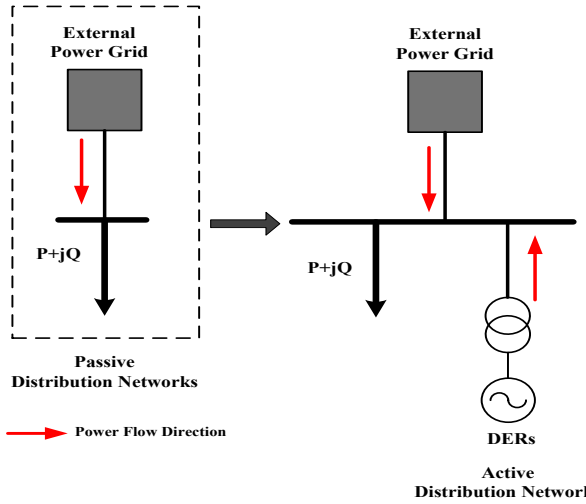

Figure 4-4 A Comparison of Passive and Active Distribution Networks

4.4 Simulation Results

In order to estimate the interaction between the distributed wind energy generator with electric charging station in the proposed active distribution network. Case study is carried out in the chosen regional distribution network as shown in Fig. 4-5. Assuming this is a residential district with wind generators. Charging stations are installed for those electric vehicles based on owner's fast-charging requirements.

Simulations were carried out on the distribution grid with a wind turbine and a charging station in Figure 4-5 where the wind generator is connected with B1. Using the test system, three cases were carried out as follows:

Case 1: A three phase ground fault is applied at B2 and cleared 1s later. In this case, no charging station is installed;

Case 2: A three phase ground fault is applied at B2 and cleared 1s later. In this case,

a charging station is installed at B5;

Case 3: Similar to Case 2 except that the charging station is installed at B6;

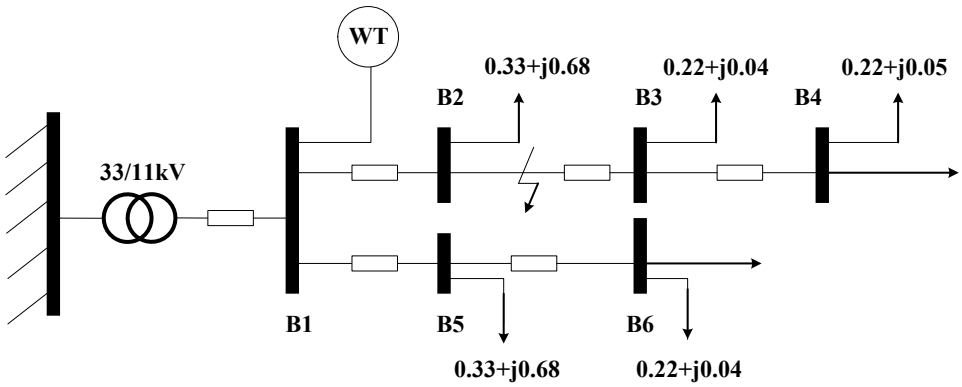

Figure 4-5 Test Electricity Distribution Grid (load in MW)

Figure 4-6 shows the voltage profile measured at B1 in Case 1. At time 0.5s, three-phase ground fault was applied at B2, and fault was cleared 0.1s later, a distinctive voltage dip can be observed from Figure 4-6, where the fault is extremely severe such that the voltage falls below 0.15 p.u., which is below the limit specified in the grid code issued by the UK National Grid Company [64]. The voltage limit specified by the Grid Code is shown with dotted line in Figure 4-6. In this situation, the wind generator was tripped and disconnected from the distribution grid due to the large voltage dip.

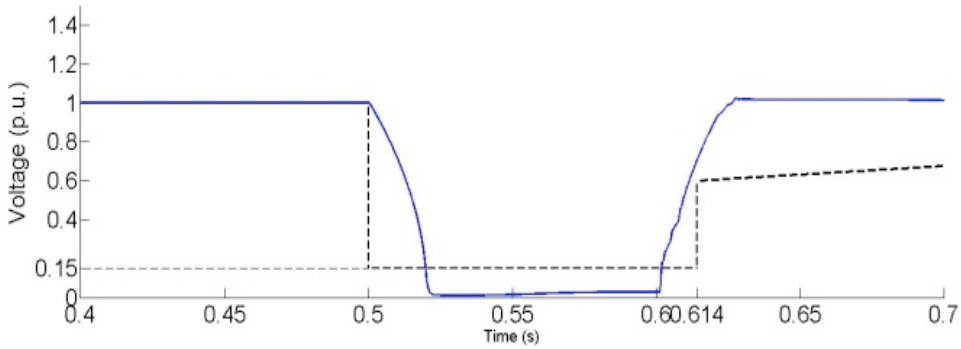

Figure 4-6 Voltage Profile at B2 with no Charging Station Installed

In Case 2, the charging station is installed at B5 in the local residential district. When the fault is applied at B2, because of the charging station has the ability to transfer power from the electric vehicle battery to the grid, when the battery voltage is above the voltage of the connection point. The voltage at B1 can be maintained above its limit, as shown in Figure 4-7. Under the circumstances, the electric vehicle battery is operating as a distributed energy source that injects power to the grid.

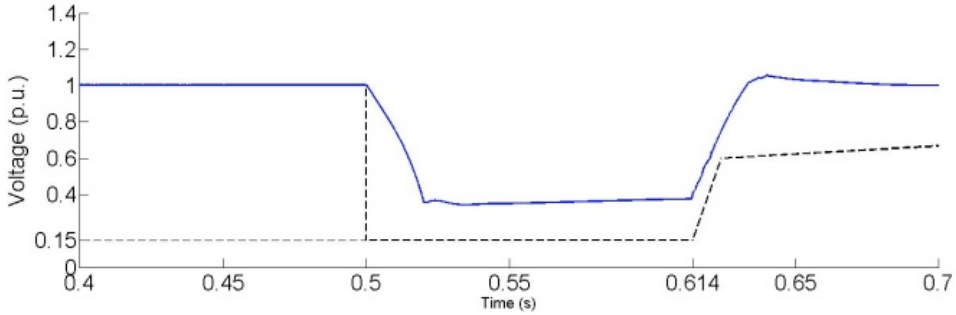

Figure 4-7 Voltage Profile at Bus 2 with Charging Station Installed at Bus 5

A further case study carried out by installing the charging station at a different location within the test distribution system. In Case 3, the charging station is installed at B6. Voltage profile measured at B1 is shown in Figure 4-8. When the fault occurred at B2 at 0.5s, the voltage fell to 0.2 p.u, which is still above the bus voltage limit given by the Grid Code, and then the fault was cleared at time 0.6s and after this, the voltage was recovered.

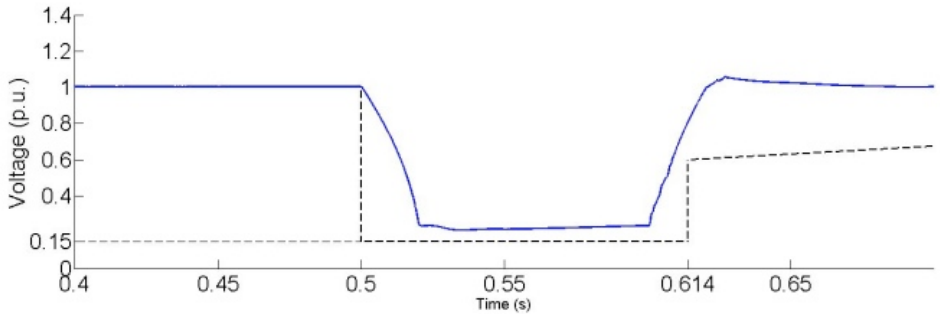

Figure 4-8 Voltage Profile at Bus 2 with Charging Station Installed at B6.

4.5 Summary

This Chapter has examined that EV charging stations with bi-direction power flow control capability can provide the voltage support for distribution network operations to improve the fault-ride-through of adjacent wind turbines. Simulations have illustrated the feasibility as well as the effectiveness of the proposed control concept. Hence such voltage support from EV charging station has the great potential to be developed as ancillary services in smart distribution grid operations.

Chapter 5 Conclusions and Future Work

5.1 General Conclusions

This thesis consists of two parts; the first part is on the modeling of electric vehicle charging station. And the second part of this thesis was investigating the bi-directional power transfer between electric vehicle and grid. Detailed conclusions are demonstrated below:

1. The equivalent model of electric batteries has been developed and implemented in MATLAB. The model has been used to evaluate the terminal voltage and power variation during the battery charging and discharging periods. The concept of electric vehicle fast charging station has been summarized and its detailed simulation model has been designed to integrate the electric vehicle batteries with the distribution network.

2. The modeling of a wind turbine with DFIG has been presented. As a wind generator requires the fault ride-through ability, crowbar protection was considered in the simulation model. As the simulation results have shown that the crowbar protection allows fault ride-through for the DFIG wind turbine, if the DC-link capacitor voltage is contained within an acceptable limit. The function of the crowbar is to dissipate the excess active power and prevent the DC-link capacitor voltage from unnecessary increase, which may lead to a higher rotor current through the RSC.

3. The interactions between electric vehicle charging stations and active distribution

grid have been investigated, which is considered to be the major contribution of this thesis. This Chapter has examined that EV charging stations with bi-direction power flow control capability can provide the voltage support for distribution network operations to improve the fault-ride-through of adjacent wind turbines. Simulations have illustrated the feasibility as well as the effectiveness of the proposed control concept. Hence such voltage support from EV charging station has the great potential to be developed as ancillary services in smart distribution grid operations.

5.2 Future Work

In regarding the topics in this research, it is necessary to do further study on the following aspects:

- The simulation model for the electric vehicle battery and charging station is mainly developed for power grid transient analysis. Further models will be needed for long term simulations where the charging cycle and some other battery parameters should be considerate in the model.

- The analysis of the interaction between electric vehicles and distribution grid should be enhanced to include other types of distributed generators (DGs) including CHPs, PVs, and energy storage devices, etc.
- The simulation work was developed in Matlab/Simulink, future simulation work will need to migrate to some other advanced power system simulation

software packages, with more rich DG simulation models and for large scale power grid simulations.

- Researches on commercial frameworks for ancillary services from EVs can be developed, future researches will need to investigate the demonstration projects of EV commercial developing worldwide, building commercial frameworks for ancillary services based on local situation.

References

[1] S. Newman, *The final energy crisis, 2nd Edition*. London: Pluto Press, 2008.

[2] H. Michael and K. Snorre, "Depletion of fossil fuels and the impacts of global warming," *Resource and Energy Economics*, vol. 18, no. 2, pp. 115-136, Jun. 1996.

[3] European Wind Energy Association, *Wind energy - The facts*. London: Earthscan, 2009.

[4] E. Ungar and K. Fell, "Plug in, turn on, and load up," *IEEE Power and Energy Magazine,* vol. 8, no. 3, pp. 30-35, May 2010.

[5] A. K. Srivastava, B. Annabathina, and S. Kamalasadan, "The challenges and policy options for integrating plug-in hybrid electric vehicle into the electric grid," The Electricity Journal, vol. 23, no. 3, pp. 83-91, Mar. 2010.

[6] D. Sperling, and G. Deborah, *Two billion cars: driving toward sustainability*, New York: Oxford University Press, 2009.

[7] D. B. Sandalow, *Plug-in electric vehicles: what role for washington?* Washington: The Brookings Institution, 2009.

[8] E. Ungar and K. Fell, "Plug in, turn on, and load up," *IEEE Power and Energy Magazine*, vol. 8, 2010, pp. 30-35.

[9] Tingting Zhao, *China accelerates electric vehicle dream*, August, 2010, at http://www.chinadaily

[10] JD Power & Associates. “Drive green 2020: more hope than reality?” November 2010.

[11] http://www.chargepointamerica.com/

[12] http://www.theevproject.com/

[13] X.K. Lai, “Impact of electric vehicles on the power grid,” http://www.gmexpo2010.com/downloads/forum/20100727%20Lai's%20Presentation.pdf

[14] http://www.delta-ee.com/downloads/RESEARCH_BRIEF_French%20EV%20plan_SHOct09.pdf

[15] http://urbact.eu/fileadmin/Projects/EVUE/documents_media/London_presentation_Feb_2010.pdf

[16] R. D. Richardson and G. M. Mcnerney, “Wind energy systems,” *Proceedings of the IEEE*, vol. 81, no. 3, pp. 378-389, Mar. 1993.

[17] P. Musgrove, Wind energy, Cambridge: Cambridge University Press, 2009.

[18] World Wind Energy Association Head Office, *World wind energy half-year report 2011*, World Wind Energy Association, Tech. Report, Aug. 2011.

[19] RenewableUK, “UK wind energy database statistics,” March 2012, [Online]. Available: http://www.bwea.com/statistics/.

[20] Y. Wu, *Research on reliability evaluation and expansion planning of power system including wind farms*, Ph.D. dissertation, School of Electric Engineering, Hefei University of Technology, Hefei, Anhui, China, 2006.

[21] Z. Hu, Y. Song, Z. Xu, et al., "Impacts and utilization of electric vehicles into power systems," *Proceedings of the CSEE*, vol. 32, no. 4, pp. 1-11, Feb. 2012.

[22] C. Gao and L. Zhang, "A Survey of influence of electrics vehicle charging on power grid," *Power System Technology*, vol. 35, no. 2, pp. 127-131, Feb. 2011.

[23] A. K. Srivastava, B. Annabathina, and S. Kamalasadan, "The challenges and policy options for integrating plug-in hybrid electric vehicle into the electric grid," *The Electricity Journal*, vol. 23, no. 3, pp. 83-91, Apr. 2010.

[24] T. H. Bradleya and A. A. Frankb, "Design, demonstrations and sustainability impact assessments for plug-in hybrid electric vehicle," *Renewable and Sustainable Energy Reviews*, vol. 13, no. 1, pp. 115-128, Jan. 2009.

[25] S. S. Williamson, "Electric drive train efficiency analysis based on varied energy storage system usage for plug-in hybrid electric vehicle," in *Proceedings of 2007 IEEE Power Electronics Specialists Conference*, Orlando, FL, USA, pp.1515-1520, Jul. 17-21 2007.

[26] G. T. Heydt, "The Impact of electric vehicle deployment on load management strategies," *IEEE Transactions on Power Apparatus & System*, vol. 1, no. 144, pp. 1253-1259, May 1983.

[27] A. Heider and H. J. Haubrich, "Impact of wide-scale ev charging on the power supply network," in *Proceedings of IEE Colloquium on Electric vehicles: A Technology Roadmap for the Future*, London, UK, vol. 6, no. 262, pp. 1-4, May 5 1998.

[28] K. Schneider, C. Gerkensmeyer, M. Kintner-Meyer, and M. Fletcher, "Impact assessment of plug-in hybrid electric vehicles on pacific northwest distribution systems," in *Proceedings of 2008 IEEE Power and Energy Society General Meeting*, Pittsburgh, PA, USA, pp. 1-6, Jul. 20-24 2008.

[29] K. Mets, T. Verschueren, W. Haerick, and etc., "Optimizing smart energy control strategies for plug-in hybrid electric vehicle charging," in *Proceedings of 12th IEEE/IFIP Network Operations and Management Symposium Workshops*, Osaka, Japan, pp. 293-299, Apr. 19-23 2010.

[30] N. Rotering and M. Ilic, "Optimal charge control of plug-in hybrid electric vehicles in deregulated electricity markets," *IEEE Transactions on Power Systems*, vol. 26, no. 3, pp. 1021-1029, Aug. 2011.

[31] W. Kempton and J. Tomic, "Vehicle-to-Grid power implementation: from stabilizing the grid to supporting large-scale renewable energy," *Journal of Power Sources*, vol. 144, no. 1, pp. 280-294, Jun. 2005.

[32] H. Turton and F. Moura, "Vehicle-to-Grid systems for sustainable development: an integrated energy analysis," *Technological Forecasting and Social Change*, vol. 75, no. 8, pp. 1091-1108, Oct. 2008.

[33] C. Guille and G. Gross, "A conceptual framework for the vehicle-to-grid (V2G) implementation," *Energy Policy*, vol. 37, no. 11, pp. 4379-4390, Nov. 2009.

[34] W. Kempton and J. Tomic, "Vehicle-to-grid power fundamentals: calculating capacity and net revenue," *Journal of Power Sources*, vol. 144, no. 1, pp. 268-279, Jun. 2005.

[35] M. Etezadi-Amoli, K. Choma, and J. Stefani, "Rapid-charge electric-vehicle stations," *IEEE Transactions on Power Delivery*, vol. 25, no. 3, pp. 1883-1887, Jul. 2010.

[36] J. Taylor, A. Maitra, M. Alexander, D. Brooks, and M. Duvall, "Evaluation of the impact of plug-in electric vehicle loading on distribution system operations," In *Proceedings of IEEE PES Power & Energy Society General Meeting* 2009.

[37] E. Sortomme, M. Hindi, "Coordinated charging of plug-in hybrid electric vehicles to minimize distribution system losses." *IEEE Transaction on Smart Grid*, vol.2, no.1, March 2011.

[38] S. Shao, M. Pipattanasomporn, and S. Rahman, "Challenges of electric vehicle penetration to the residential distribution network," *2009 IEEE PES General Meeting*, 2009, paper 09GM0514, pp. 1–8.

[39] A. Maitra, K. S. Kook, A. Giumento, J. Taylor, D. Brooks, M. Alexander, and M. Duvall, "Evaluation of PEV loading characteristics on Hydro-Quebecs distribution system operations," *PHEV09*, Montreal, 28- 30 September 2009.

[40] D. Linden, and T. B. Reddy, , (editors), *Handbook of Batteries*, 3rd edition, McGraw-Hill, New York, NY, 2001.

[41] P. Bauer, N.Stembridge, J. Doppler, , and P. Kumar, "Battery modeling and fast charging of EV", *14th International Power Electronics and Motion Control Conference, EPE-PEMC*, 2010

[42] H.W. Kim, S.S Kim, H.S. Ko, "Modeling and control of PMSG based variable speed", *Electric Power Systems Research*, vol.11, no 1, pp. 147-154, October, 2009

[43] Y. Chen, A. Oudalov, J. S. Wang, "Integration of electric vehicle charging system into distribution network", *8th International Conference on Power Electronics – ECCE Asia*. Beijing, China, 2010

[44] M. Chen and G. A. Rincon-Mora, "Accurate electrical battery model capable of predicting runtime and I-V performance," *IEEE Trans. Energy Conversion*, vol. 21, no. 2, pp. 504-511, June 2006.

[45] M. Knauff, et. al, "Simulink model of a lithium-ion battery for the hybrid power system testbed," *Proceedings of the ASNE Itelligent Ships Symposium*, Philadelphia, PA, USA, May 2007.

[46] O. Erdinc, B.Vural, and M. Uzunoglu, "A dynamic lithium-ion battery model considering the effects of temperature and capacity fading," *2009 International Conference on Clean Electric Power*, Capri, Italy, 9-11 June 2009.

[47] A123 Systems Hymotion Products http://www.a123systems.com/-hymotion/products/N5_range_extender.

[48] M.C. Kisacikoglu, B. Ozpineci, L.M. Tolbert, "Examination of a PHEV bidirectional charger system for V2G reactive power compensation," *Applied Power Electronics Conference and Exposition (APEC)*, Florida, US. 21-25 Feb. 2010

[49] S. Muller, M. Deicke, R.W. De Doncker "Doubly fed induction generator systems for wind turbines", *IEEE Industry Application Magazine*, vol. 8, no. 3, pp. 26-33

[50] V. Akhmatov, "Variable-speed wind turbine with doubly-fed induction generators –Part I: modelling in dynamic simulation tools", *Wind Energy*, vol. 26, no. 2, pp. 85-108

[51] T. Petru, T. Thiringer, "Modeling of wind turbines for power system studies," *IEEE Trans. on Power Systems*, vol.17, no. 4, 2002, pp.1132-1139

[52] A. Pertersson, T. Thiringer, L. Harnefors, et al. "Modeling and experimental verification of grid interaction of a DFIG wind turbine," *IEEE Trans. on Energy Conversion,* vol.20, no.4, 2005, pp.878-886.

[53] A. Mullance, M. O'Malley , "The inertial response of induction-machine-based wind turbine," *IEEE Trans. on Power Systems*, vol.20, no.3, 2005, pp.1496-1503

[54] J. Morren, S.W.H. de Haan , "Short-circuit current of wind turbine with doubly fed induction generator," *IEEE Trans. on Energy Conversion*, vo.22, no.1, 2007, pp.174-180

[55] J.G. Slootweg, H. Polinder, W.L. Kling, "Reduced-order modelling of wind turbine", In Ackermann, T. (ed.) *Wind Power in Power Systems*. Wiley, England. 2005, pp.555-585

[56] Y. Lei, A. Mullane, G. Lightbody, et al, "Modeling of the wind turbine with a doubly fed induction generator for grid integration studies," *IEEE Trans. on Energy Conversion,* vol.21, no.1, 2006, pp.257-264

[57] F. Mei, B.C. Pal, "Modelling and small-signal analysis of a grid connected doubly-fed induction generator," in *Proceeding of IEEE PES General Meeting* 2005, San Francisco, USA, 12-16 June 2005

[58] J.G. Slootweg, W.L. Kling, "Aggregated modelling of wind parks in power system dynamics simulations," *Proceeding of 2003 IEEE PowerTech Conference*, Bologna, Italy, 23-26 June 2003

[59] P. Kundur, *Power system stability and control*, McGraw Hill, New York

[60] http://www.nationalgrid.com/NR/rdonlyres/67374C36-1635-42E8-A2B8-B7B8B9AF2408/54093/Z_CompleteGridCode_I4R14.pdfMullance A, O'Malley M (2005)

[61] A. Mullance, O. Malley, "The inertial response of induction-machine-based wind turbine," *IEEE Trans. on Power Systems*, vol.20, no.3, pp.1496-1503, 2010

[62] M. Yamamoto, O. Motoyoshi, "Active and reactive power control for doubly-fed wound rotor induction generator," *IEEE Trans. on Power Electronics*, vol.6, no.4, 1991, pp.624-629

[63] V. Akhmatov, *Induction Generators for Wind Power*, Multi-Science Publishing Company, Ltd., 2005.

[64] W. Kempton and J. Tomic, “Vehicle-to-grid power implementation:From stabilizing the grid to supporting large-scale renewable energy,” *J. Power Source*s, vol. 144, pp. 280–294, Jun. 2005.

[65] J.R. Pillai and B. Bak-Jensen, "Integration of vehicle-to-grid in the western danish power system," *IEEE Transactions on Sustainable Energy*, vol. 2, pp. 12-19, 2011.

[66] N. Mohan, T.M. Undeland and W. P. Robbins, *Power electronics converters, applications, and design*, Wiley India Press (p.) Ltd. Third Edition, Reprint 2009.

[67] H.W. Kim, S.S Kim, H.S. Ko, “Modeling and control of PMSG based variable speed,” Electric Power Systems Research, October, 2009

[68] E.J. Couster, J.M.A. Myrzik, “Integration issues of distributed generation in distribution grids,” *Proceedings of the IEEE*, vol. 99, no. 1, pp.28-39, September, 2010

[69] http://www.nationalgrid.com/NR/rdonlyres/67374C36-1635-42E8-A2B8-B7B8B9AF2408/54093/Z_CompleteGridCode_I4R14.pdf

Appendix Simulation System Configuration and Parameters

A.1Simulation Configuration for Chapter 2

A.1.1 System Simulation Configuration

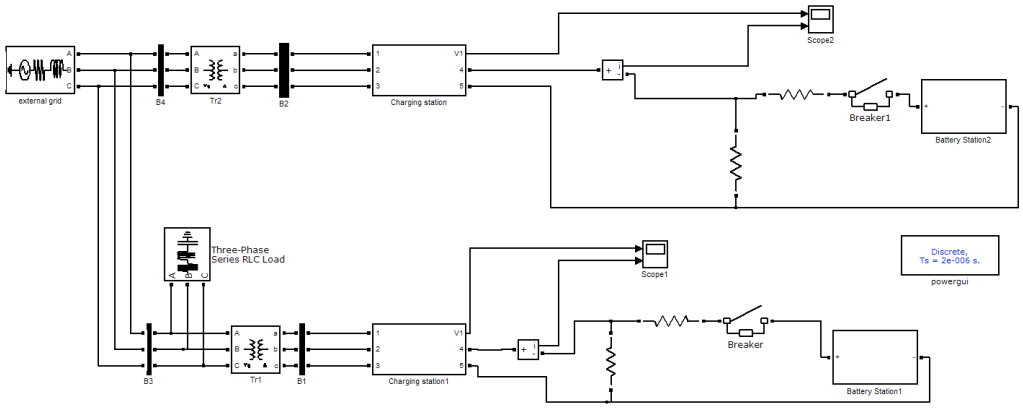

A.1.2 Charging Station Simulation Configuration.

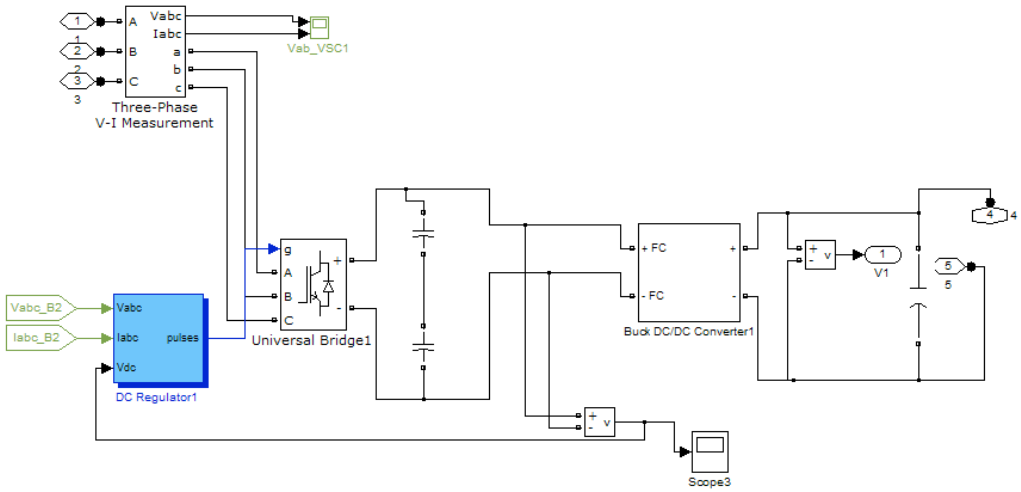

A.1.3 System Parameters

External grid	Base voltage	33kV

	Maximum voltage	1.03 pu
	Minimum voltage	0.97 pu
Load	Reactive power	0.0749 MVAr
	Active power	0.392 MW

A.2Simulation Configuration for Chapter 3

A.2.1 System Simulation Configuration

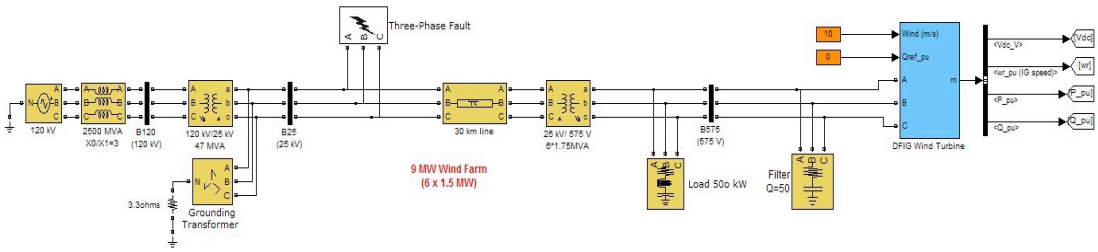

A.2.2 System Parameters

System base voltage	25kV
Transformer	25/0.575kV,
Rated capacity	12MVA
Wind farm capacity	6*1.5 MW

A.3Simulation Configuration for Chapter 4

A.3.1 System Simulation Configuration

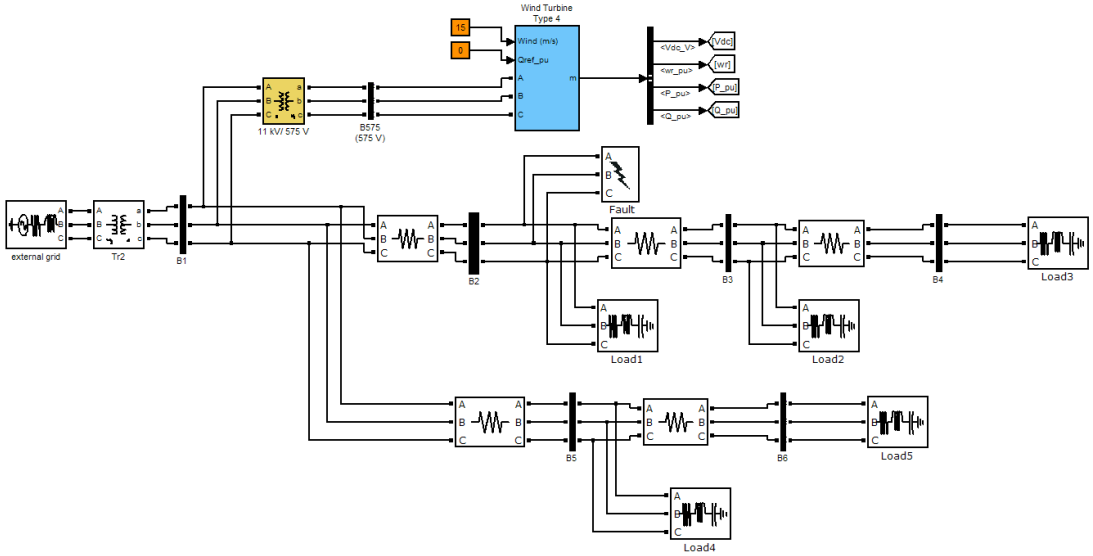

A.3.2 Charging Station Configuration

A.3.2.1 AC-DC Rectifier Diagram

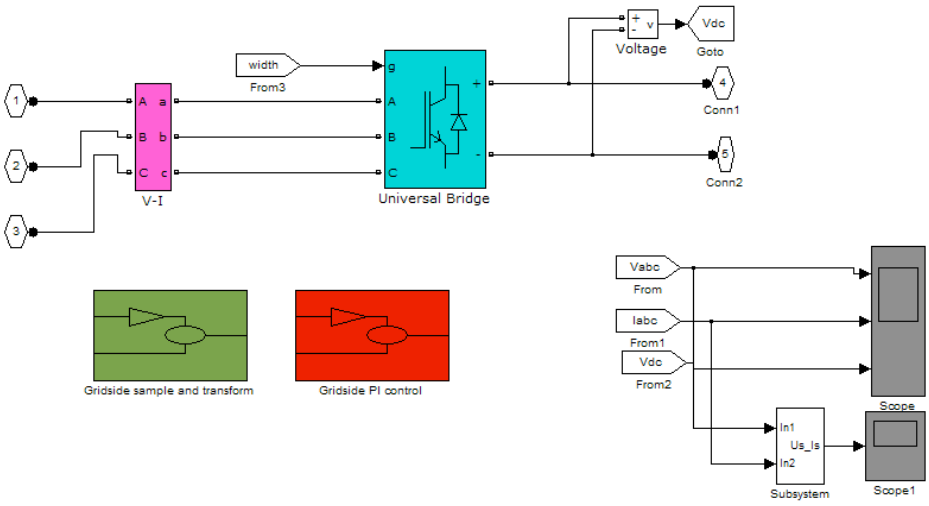

A.3.2.2 Grid Side PI Controller

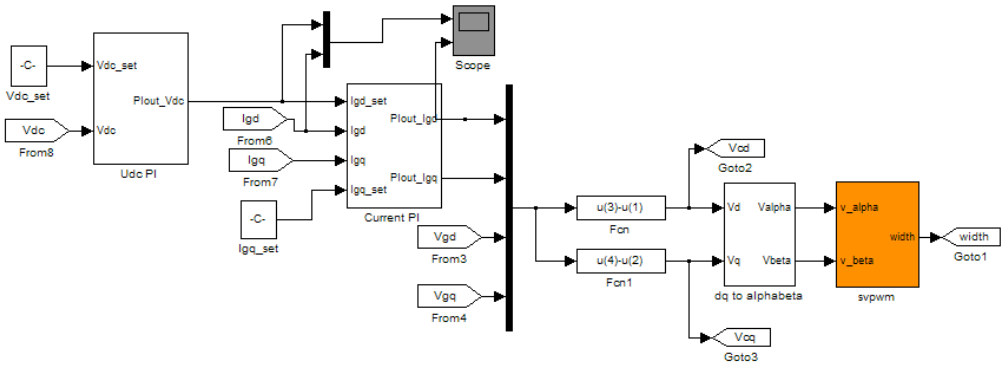

A.3.2.3 Bi-directional DC-DC Converter and its Control Diagram

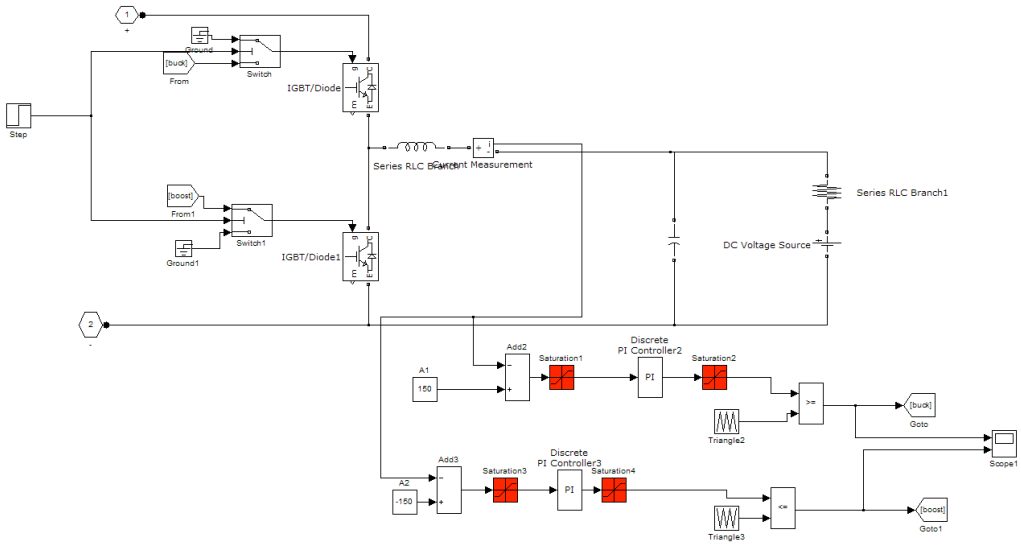

A.3.3 System Parameters

A.3.3.1 External Grid and Transformer Data

External Grid	Base voltage	33kV
Transformer	Positive and negative sequence resistance	0.047 pu
	Positive and negative sequence reactance	0.654 pu
	Zero sequence resistance	0.555 pu
	Zero sequence reactance	0
	Winding connection	YD11
Load (in MW/MVA)	Load 1	0.33+j0.68
	Load 2	0.22+j0.04
	Load 3	0.22+j0.05
	Load 4	0.33+j0.68
	Load 5	0.22+j0.04

A.3.3.2 Distribution Grid Data (in Per Unit)

From Bus	To Bus	Positive and negative	Positive and negative	Zero sequence	Zero sequence	Length (km)

		sequence resistance	sequence reactance	resistance	reactance	
Bus 1	Bus 2	0.2038	0.1056	0.6028	0.1014	1.504
Bus 2	Bus 3	0.2038	0.1056	0.6028	0.1014	0.500
Bus 3	Bus 4	0.0624	0.0170	0.1665	0.0170	0.236
Bus 1	Bus 5	0.2038	0.1056	0.6028	0.1014	1.504
Bus 5	Bus 6	0.2038	0.1056	0.6028	0.1014	0.511

List of Publications

[1] R. Shi, X.P. Zhang, et al, "Dynamic impacts of fast-charging stations for electric vehicles on active distribution networks," *in Proceedings of 2012 IEEE Conference on Innovative Smart Grid Technologies - Asia (ISGT Asia)*, Tianjin, China. May. 20-24, 2012.

[2] R. Shi, X.P. Zhang, "Support of Wind Turbine Operations in Electricity Distribution Grid by Electric Vehicles Charging Stations," *IEEE Transaction on Power & Energy Letters. Submitted.*